Atmos. Chem. Phys., 22, 13581–13605, 2022
https://doi.org/10.5194/acp-22-13581-2022

Atmospheric Chemistry and Physics
Open Access
EGU

Circular polarization in atmospheric aerosols

Santiago Gassó[1,2] and Kirk D. Knobelspiesse[3]

[1]ESSIC, University of Maryland, College Park, MD 20740, USA
[2]Code 613, Climate and Radiation Laboratory, GSFC/NASA, Greenbelt, MD 20771, USA
[3]Code 616, Ocean Ecology Laboratory, GSFC/NASA, Greenbelt, MD 20771, USA

Correspondence: Santiago Gassó (santiago.gasso@nasa.gov)

Received: 19 January 2022 – Discussion started: 17 March 2022
Revised: 19 August 2022 – Accepted: 12 September 2022 – Published: 20 October 2022

Abstract. Recent technological advances have demonstrated the feasibility of deploying spaceborne optical detectors with full polarimetric capabilities. The measurement of all four Stokes coefficients opens significant new opportunities for atmospheric aerosol studies and applications. While considerable amounts of attention have been dedicated to sensors with sensitivity to the total intensity and linear polarization (represented by Stokes coefficients I, U, Q), there has been less attention to the additional information brought by measuring circular polarization (coefficient V). This report fills this gap in knowledge by providing an overview of aerosol sources of circular polarization in the atmosphere and discusses possible remote sensing signatures.

In this paper, circularly polarized radiation that results from the interaction of incident unpolarized radiation is considered in three physical settings: optical activity originating in biogenic aerosols, alignment of non-spherical particles in the presence of electrical fields (such as dust, smoke, and volcanic ash), and aerosol multiple scattering effects. Observational and theoretical evidence of, and the settings and conditions for, non-zero aerosol circular polarization generated from incident unpolarized radiation are here gathered and discussed. In addition, novel radiative transfer simulations are shown to illustrate notable spectral and other features where circular polarization may provide additional information that is possibly independent from total intensity and linear polarization-only observations.

Current techniques for the detection of aerosol composition (also referred as aerosol type) from space provide limited information. Remote identification of aerosols such as smoke, volcanic ash, and dust particles can only be accomplished with some degree of confidence for moderate to high concentrations. When the same aerosols are found at lower concentrations (but still high enough to be of importance for air quality and cloud formation), these methods often produce ambiguous results. The circular polarization of aerosols is rarely utilized, and we explore its value for improved determination aerosol composition. This study is presented as an overview with a goal to provide a new perspective on an overlooked optical property and to trigger interest in further exploration of this subject.

1 Introduction

The 1970s were an important decade from the viewpoint of polarimetric remote sensing. The planetary probes Pioneer 10, 11, and 12 surveyed the planets Venus and Jupiter with a full polarimetric sensor (that is, a sensor capable of measuring all four Stokes parameters) (Murdin, 2001; NASA, 2021). Since then, no similar probe has been deployed for atmospheric planetary observations. In contrast, technologies based on multispectral (and later multiangle) remote sensing of total intensity have made considerable strides and have been the cornerstone for the current era of global planetary observations of aerosols with passive sensors. The last 20 yr have shown a significant amount of progress in the global quantification of aerosol concentration from space. Passive imagers with observing bands from the near ultraviolet (UV) to the infrared (IR) range (such as the sensors MODIS/VIIRS, OMI/TropOMI) routinely obtain a global daily distri-

bution of aerosols. The detection methodology is indirect in that measured radiances are analyzed via a complex modeling approach to derive an aerosol optical depth (AOD, representing atmospheric column light extinction) which serves as a proxy of the total aerosol concentration. With this retrieved quantity, it is now possible to quantify with satellite observations the total amount of atmospheric aerosols globally. Aerosol global transport models now have such observations available and are used to constraint model initializations or validate model outputs. In addition, they contribute to more focused and applied decision-making fields such air quality and public health (Duncan et al., 2014; Holloway et al., 2021; Mhawish et al., 2018; Sorek-Hamer et al., 2020; Wei et al., 2020).

A notable feature is the discrepancy between the level of compositional aerosol diversity in aerosol models and remote sensing-derived aerosol properties. Aerosol transport models tend to simulate 4–6 aerosol tracers frequently labeled according to their source type, namely smoke, dust, and others (Colarco et al., 2010; Inness et al., 2019), whereas transport models with more chemical transformation focus tend to group aerosol types according to composition such as sulfur, soot, etc. (Bian et al., 2017; Binkowski and Roselle, 2003). The convergence of these descriptions can be facilitated by observations, and thus the identification of aerosols from space provides an important observational constraint to aid aerosol modeling efforts. Standard aerosol detection techniques can identify several aerosol types (here interpreted as a proxy for aerosol composition) such as smoke, dust, volcanic ash, and pollution aerosols (Kahn and Gaitley, 2015; Z. Li et al., 2019; Mhawish et al., 2018). However, an important aerosol group is not detected by these techniques: biogenic organic aerosols (BOAs). These are a subset of a larger group (organic aerosols) and are sourced from precursor gases generated by biogenic activity (e.g., isoprene from forests) or actual biological remains (dead or live bacteria, fungi, spores) injected in the atmosphere (Facchini et al., 2008; Leck and Bigg, 2005; Sanchez et al., 2018; Verdugo et al., 2004). BOAs are an important component in the global aerosol budget (Myriokefalitakis et al., 2017) and the contribution to the total aerosol budget is poorly constrained (Alsante et al., 2021). Not only they are effective cloud condensation nuclei (CCN) and ice nuclei particles (Després et al., 2012; O'Dowd et al., 2004; Twohy et al., 2021) but they can be the dominant aerosol in remote marine and tropical environments (McCoy et al., 2015). Notably, there are very few surveys of the abundance of BOA in organic matter aerosols but recent reports highlight their importance in the aerosol budget (Hodzic et al., 2016; Samaké et al., 2019) and their presence throughout the atmospheric column (Perring et al., 2014). They can also be transported long distances and contribute to the intercontinental transport of pathogens (Kellogg and Griffin, 2006).

Current retrieval schemes based on spectral variability of the observed total radiance can confidently distinguish between smoke and dust at moderately to very highly polluted conditions (AOD (500 nm) $> \sim 0.2$–0.3). However, differentiation of the two types can yield mixed results at moderate concentration levels ($\sim 0.12 <$ AOD $< \sim 0.23$), and detection is highly unreliable at background conditions (AOD < 0.12). These thresholds are approximate because detection effectiveness is highly dependent on the retrieval assumptions such as surface type and the cloud removal scheme. However, this picture arises from the validation efforts by the different algorithm development teams when trying to compare satellite aerosol type proxies as function of aerosol loading with independent observations (Ahn et al., 2014; Franklin et al., 2017; Jethva et al., 2014; Jethva and Torres, 2019; Sayer et al., 2013, 2018; Schutgens et al., 2021). The inadequate detection of aerosol type at moderate and background concentration of aerosols constitutes an important limitation. For example, aerosols with different composition such as biological or sea-salt-dominated aerosol in the pristine marine environment (i.e., background conditions) can have very different impacts on cloud formation (Moore et al., 2013). Thus, having the ability to distinguish between the two would provide important information for cloud model parameterizations and understanding of the evolution of cloud formation in vast areas of, for example, the Southern Ocean. Furthermore, aerosol type discrimination (for example, between pollen, smoke, and dust) at moderate concentration levels is also very important for public health (Magzamen et al., 2021; Manisalidis et al., 2020). These are features shared by most retrieval schemes using multispectral passive sensor with a single view, such as the algorithms applied to MODIS and VIIRS (Hsu et al., 2013; Levy et al., 2013).

There are, however, more sophisticated sensors that have better aerosol-type detection capabilities. For example, angular variability of the spectral radiance (MISR, Diner et al., 2005), active remote sensing (CALIOP, Winker et al., 2010), and polarization (POLDER, Herman et al., 2005; L. Li et al., 2019) are used to better discriminate between aerosol types, but other technical impediments (limited spatial coverage, adequate pixel size) prevent an effective global coverage. Two sensors (POLDER and CALIOP) are highlighted as the first operational sensors to make observations of linearly polarization (LP) of the Earth surface–atmosphere system. The addition of (linear) polarization capabilities provides for improved determination of aerosol optical properties as a proxy for composition (Knobelspiesse et al., 2012). Particle complex refractive index and particle shape have been successfully used to determine aerosol types where polarization-insensitive methods have fallen short (Dubovik et al., 2011; Omar et al., 2009; Russell et al., 2014; Stamnes et al., 2018). Like those that use intensity-only passive sensors, the capability of these remote sensing techniques depend on the amount of aerosols, and are less effective for aerosol type identification in low-to-moderate loading conditions.

A notable feature in existing and planned remote sensing sensors onboard satellite platforms using polarization technologies is that they do not capture all possible optical information from observed upwelling radiances. Specifically, full optical information in an atmospheric signal is represented by the four Stokes components: (1) total radiance (labeled I) is what most passive spectral imagers measure; (2) linearly polarized radiances (represented by two components U and Q) such as those used in currently operational (POLDER, CALIOP) and planned (MAIA, HARP2, SPEXone) sensors (Hasekamp et al., 2019; Liu and Diner, 2016; Remer et al., 2019); and (3) circularly polarized radiance (V). While significant attention has been dedicated to studies involving total intensity and linear polarization, there is a notable dearth of theoretical and observational atmospheric studies focusing on aerosol information contained in the circular polarization (CP) associated with the fourth Stokes element. Much of the seminal work on atmospheric propagation of CP was carried out in the 1970s (Coffeen, 1979; Hansen, 1971; Hansen and Hovenier, 1974; Kawabata et al., 1980; Kawata, 1978) to study the cloudy atmospheres of Jupiter and Venus. However, no additional dedicated work has been carried out afterwards particularly in the context of Earth's atmosphere.

Until recently, the conventional wisdom relied on modeling studies showing that CP is present in multiple scattering environments such as in clouds (Kawata, 1978) or dense smoke clouds (Slonaker et al., 2005). In a multiple scattering setting, the first scattering event generates linearly polarized light (LP) and a particle will scatter circular polarized light in the second scattering event regardless of the particle shape. The magnitude of degree of CP polarization (a common metric for evaluation, defined as $\mathrm{DCP} = V/I$) can be significantly lower than the degree of linear polarization with values in the 10^{-2} to 10^{-5} range. Its low range has been a challenging requirement for Earth-observing sensors that have exposure times of the order of milliseconds as opposed to planetary probes that had much coarser spatial resolutions and longer exposure times. Sensor sensitivity and lack of a compelling scientific application have been the main reasons to justify the lack of inclusion of CP observation in spectro-polarimeters to be deployed in the near future (Craven-Jones et al., 2014; Dubovik et al., 2019; Stamnes et al., 2021; Trippe, 2014). Interestingly this fact was already raised by Kemp et al. (1971) who noted that the "the appreciable linear polarization of the planets ... had discouraged a search for any circular polarization, which is expected to be much smaller than the linear component".

Innovations in polarimetric hardware and technology now make feasible the deployment of imagers with full-Stokes radiance measurement capabilities (Lucas Patty et al., 2019b; Rubin et al., 2019; Sparks et al., 2019b) with much easier to deploy and smaller hardware enclosures. This new generation of sensors raises the possibility that in the not-so-distant future there may be a deployment of an Earth-looking sensor with full polarimetric observing technologies. Concurrent with these hardware advances, there has been significant scientific progress in the characterization of polarimetric properties of aerosols. These two developments prompt revisiting the utility of circular polarization from aerosols. Thus, the purpose of this report is to summarize these recent scientific developments and highlight relevant CP features that can be used for better identification of aerosols by remote sensing means, particularly from space. Specifically, three circumstances are identified where circular polarization is produced in the interaction of sunlight with (1) aerosols with chiral molecules (such as pollen and other biogenic aerosols); (2) aligned non-spherical particles such as those in electric field created within dust, smoke, and volcanic ash clouds; and (3) high concentration aerosols where multiple scattering conditions are present.

This report is structured as follows. Sections 2 and 3 give introductory information useful for the interpretation of the rest of this report. Section 2 provides a brief theoretical introduction on the representation of polarization and some common assumptions used to simplify computations of polarized scattering. Section 3 introduces the concept of chirality in aerosols and their optical features. Section 4 discusses the alignment of particles in the atmosphere and how it relates to aerosol CP. Section 5 focuses on the evidence available of circular polarization in laboratory, field, and remote sensing studies. Section 6 discusses the considerations needed for studying aerosol propagation in the atmosphere and provides a modeling example of the generation of CP radiances in an ideal atmosphere. Section 7 is a summary of the main features regarding aerosol CP discussed here with suggestions for future applications and research.

2 Theoretical aspects in the representation of circular polarization

While not attempting to provide a thorough introduction, a few theoretical aspects of CP's representation in the Stokes formalism are highlighted. For excellent references on the subject, the reader is referred to some of the classic texts (Bohren and Huffman, 1998; Goldstein and Goldstein, 2003; van de Hulst, 1957) from which this section is largely adapted.

A propagating electromagnetic wave can be represented as a wave with its plane of vibration perpendicular to the direction of propagation and this wave vector can be projected onto two perpendicular axes in the same plane. The projected components of the wave in each axis can be slowed down by the solid's inhomogeneities (these inhomogeneities are expressed mathematically as a non-identity dielectric tensor). The difference in propagation speeds in each projection of the traveling wave results in changes in phase and magnitude of each of the observed components of the propagating light. The result of these differences is the elliptical polarization of light, with linear and circular polarization to be particular

cases. Polarization thus results from the differential speeds of the wave components of the traversing light. The challenge is to relate the observables (i.e., angular and spectrally dependent radiation) with the microphysical structure of the medium.

In the specific the case of incident unpolarized light, CP can arise out of the first scattering event from a single particle if the particle is chiral and oriented and non-spherical (e.g., van de Hulst, 1957). This is the scenario that presents a path for direct aerosol type identification. In addition, unpolarized light incident upon an ensemble of particles can result in outgoing CP if multiple scattering occurs in the medium regardless of the particle type, shape, and orientation. In this case, it is less clear the potential to link the observed CP with a specific aerosol type under observation. An expanded description is provided in Sects. 3, 4, and 6.

The theoretical description of the scattering process can be cast in the Stokes formalism (van de Hulst, 1957). A polarized beam is represented by the Stokes column vector. The Stokes vectors for the incident and outgoing light are related by the 4×4 scattering matrix (S) that represents the scattering medium as

$$\begin{bmatrix} I_{\text{out}} \\ Q_{\text{out}} \\ U_{\text{out}} \\ V_{\text{out}} \end{bmatrix} = \begin{bmatrix} S_{11} & S_{12} & S_{13} & S_{14} \\ S_{21} & S_{22} & S_{23} & S_{24} \\ S_{31} & S_{32} & S_{33} & S_{34} \\ S_{41} & S_{42} & S_{43} & S_{44} \end{bmatrix} \begin{bmatrix} I_{\text{in}} \\ Q_{\text{in}} \\ U_{\text{in}} \\ V_{\text{in}} \end{bmatrix}. \quad (1)$$

In an experimental setting, the incoming and outgoing light are known information and the above equation is inverted to obtain the elements of matrix **S**. These elements directly depend on particle composition, size, orientation, and shape. Composition in optical terms is expressed through the magnitude and spectral dependence of the real and imaginary part of the index of refraction. In turn, the latter is related to material elements to the particle through the dielectric matrix (if the solid is inhomogeneous) or constant (homogenous particle).

The elements S_{4j} (bottom row in Eq. 1) and S_{i4} (rightmost column) are associated to the circular polarization of the scattered light and can be used as an index to indicate the presence of CP in the observed signal (Bohren and Huffman, 1998; van de Hulst, 1957). For example, with incident unpolarized light (represented as I_{in} [1,0,0,0] in Eq. 1) onto aerosols, the system will exhibit CP if the matrix has non-zero S_{14} that result in an outgoing vector with non-zero V_{out}. From the modeling viewpoint, there are very few analytical solutions of the Maxwell's equations that provide the 16 S_{ij} coefficients. For example, exact solutions can be found for $2\pi r/\lambda << 1$ and $|mr/\lambda| << 1$ (Rayleigh scattering) with r defined as the radius of a particle, m is the particle complex refractive index with respect to the medium, and λ is the wavelength of the incident light. For larger particles, analytical solutions exist for homogenous and multilayer spheres, infinite cylinders, certain spheroids, and a handful more (Asano, 1979; Asano and Sato, 1980; Bohren and Huffman, 1998). For non-spherical particles, analytical solutions are only computationally effective for small particles due to numerical instabilities for larger particles such as semi-analytical T-matrix method, and other approximate solutions (Mishchenko et al., 2000). However, dust non-spherical particles have been successfully modeled using the discrete dipole approximation (Draine et al., 1994; Kempinnen et al., 2015) In the case of chiral particles (Sect. 3), there are exact solutions for specific particle shapes.

Another common assumption used to reduce the number of elements in matrix **S** results from the consideration of ensembles of particles. Symmetries in matrix **S** arise when all particles in the ensemble share the same composition, they are randomly oriented, or when particle shapes have mirror symmetry. These three considerations together lead to simplifications in the scattering matrix for an ensemble of particles by reducing the number of coefficients in matrix **S** (van de Hulst, 1957; Mishchenko and Yurkin, 2017; Perrin, 1942):

$$\begin{bmatrix} \text{S}_{11} & \text{S}_{12} & 0 & 0 \\ \text{S}_{12} & \text{S}_{22} & 0 & 0 \\ 0 & 0 & \text{S}_{33} & \text{S}_{34} \\ 0 & 0 & -\text{S}_{34} & \text{S}_{44} \end{bmatrix}. \quad (2)$$

This matrix has six independent elements, and it is the most common form of matrix **S** used in optical modeling studies of atmospheric aerosols and in the simulation of aerosol radiances for remote sensing applications. Additional simplifications can be achieved by assuming homogenous spheres ($S_{11} = S_{22}$, $S_{33} = S_{44}$) and specific viewing geometries such as backscattering (Mishchenko and Hovenier, 1995). Matrix 2 has been thoroughly used and validated and represents a reasonable assumption when there is no a priori knowledge of the aerosol under observation. For incident unpolarized light, the first scattering event results in linear and no circular polarized light for particles with scattering properties following Eq. (2). Conversely, when cross-polarization (proportional to S_{11}–S_{22}) is detected when measuring angular scattering, the hypothesis of a collection of isotropic spheres can be ruled out (Sect. 13.6.2 in Bohren and Huffman, 1998).

For groups of particles represented by Eq. (2), non-zero V_{out} can be obtained in the first scattering event only for incident linearly polarized light which generally is not the case for incident sunlight in the Earth's atmosphere. Linear polarized light is present in multiple scattering settings (such as in the UV range or with high aerosol loading). The first scattering event will produce linear polarization which in turn will produce circular polarization in the second scattering (this effect is further discussed in Sect. 6).

Matrix 2 assumes randomly oriented particles, a condition not fulfilled for oriented non-spherical particles. In this case, symmetry of the distribution within the volume leads to 10 independent parameters as in Eq. (3a) (Sect. 5.22 in Van de

Hults, 1981 and Eq. 15.8 in Mishchenko, 2014), namely,

$$\begin{bmatrix} S_{11} & S_{12} & S_{13} & S_{14} \\ S_{12} & S_{22} & S_{23} & S_{24} \\ -S_{13} & -S_{23} & S_{33} & S_{34} \\ S_{14} & S_{24} & -S_{34} & S_{44} \end{bmatrix}, \tag{3a}$$

$$\begin{bmatrix} S_{11} & S_{12} & S_{13} & S_{14} \\ S_{12} & S_{22} & S_{23} & S_{24} \\ S_{13} & S_{23} & S_{33} & S_{34} \\ -S_{14} & -S_{24} & -S_{34} & S_{44} \end{bmatrix}. \tag{3b}$$

Similarly, in the case of the presence of an ensemble of chiral particles with an excess of right or left particles, 10 coefficients are also needed as in Eq. (3b) (see Eq. 15.10 in Mishchenko, 2014). If the ensemble is made up of an equal number of such left and right-handed particles, the matrix reduces six non-zero coefficients as in Eq. (2).

These examples illustrate that for modeling circular polarization of an ensemble of particles, additional scattering matrix elements need to be considered. The next sections will discuss different elements of evidence showing atmospheric CP and observations of non-zero S_{i4} and S_{4j} elements.

3 An overlooked source of circular polarization: chiral aerosols

The term chiral is commonly used within the field of stereochemistry to refer to a molecule that cannot be superimposed to its own mirror image. Such molecules are called isomers or chiral (hand in Greek). The distinction is important because while the molecule and its mirror image have the same atoms and bonds, they may exhibit different chemical reactions and distinctive optical properties because of the orientation of their atoms. Non-biogenic chiral molecules are present in equal quantities of the two orientations (referred to as left or right isomers, Fig. 1), but biogenic chiral molecules are only present in one orientation, that is, there is no natural occurring molecule of the opposite orientation. The orientation in space is important because it determines how the molecule interacts with incident electromagnetic radiation. Therefore, aerosols that contain biological material also contain chiral molecules and have singular optical properties that result from the interaction with light. When unpolarized or linearly polarized light is incident on a chiral particle, it will scatter circularly polarized light (known as optical rotation) or absorb polarized light (known as circular dichroism) such that the outgoing light is circularly polarized. Such molecules are said to exhibit optical activity. A particle such as dust will not generate circularly polarized light in the first interaction with light because it is not optically active. If there are equal number of left- and right-handed molecules (referred to as racemic mixtures), the two resulting opposite circular polarizations will cancel each other. The mixtures

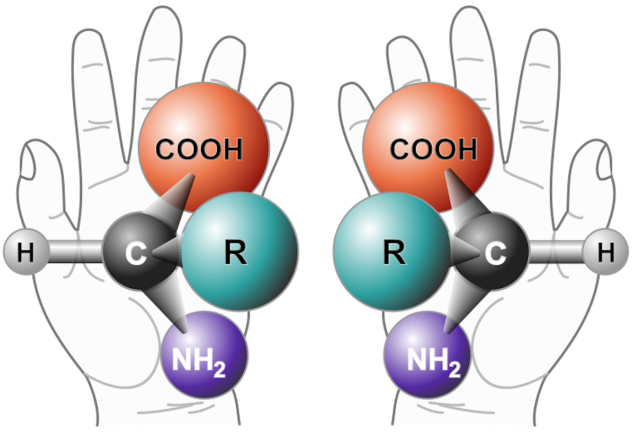

Figure 1. Two isomers (or enantiomers) of a generic amino acid, both molecules have same composition but different molecules orientation, which determines the polarization of the scattered light. Biological proteins are made of exclusively on left-handed amino acids and right-handed sugars (source: Wikipedia Commons).

with excess of one isomer can occur naturally or in synthetic compounds such as pharmaceuticals. For example, in the 1960s the use of thalidomide as a morning sickness drug by pregnant women resulted in severe birth defects. It was later found that thalidomide was a racemic mixture where the R-enantiomer had the intended sedative relief, whereas the S-enantiomer had a negative impact on fetal development (Kim and Scialli, 2011; Smith, 2009). Another example of chiral molecule is the common analgesic Ibuprofen (Shi et al., 2021): only the *S* form of the molecule is used for therapeutic applications (Evans, 2001; Neupert et al., 1997). In the natural world, chiral molecules are present in commonly found BOA such as α-pinene. A recent study (Bellcross et al., 2021) showed that different tacticity (that is, arrangement of chiral centers) of α-pinene dimers may influence its physical properties, such as hygroscopicity thus impacting cloud droplet formation (Cash et al., 2016).

There is a rich history around the discovery and development of the science of chiral molecules. Detailed summaries can be found in Barron (2009), Lakhtakia (1990), and Applequist (1987). A few historical developments in the history of optical activity are highlighted here. For example, in 1812, optical activity was first reported by Jean Batiste Biot and in 1848, Louis Pasteur established that chiral compounds have distinctive chemical properties, and its optical activity was associated with the molecule's properties. A model of the physical interaction between the incident light and a chiral molecule was first proposed in 1915 by Max Born and Carl Oseen and in parallel by Frank Gray (Applequist, 1987) . By representing the incident wave as a combination of left and right circular polarized waves (Born, 1918; Drude et al., 1902), the solutions of the scattering matrix were found by requiring two different indices of refraction to be associated to the chiral particle (one index for each right and left cir-

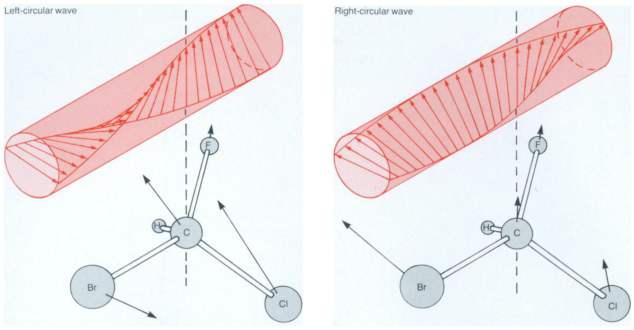

Figure 2. Illustration of the interaction of incident light decomposed in two orthogonal components (represented by the left and right circular waves) with the chiral molecule CHFClBr. As the wave moves through the molecule, it induces a dipole in each atom (arrows). The aggregate total induced dipole in the molecule is different for each incident wave, which in turn results in different refractive indices for each wave. This difference produces optical activity which can be observed in the laboratory (figure from Applequist, 1987).

cular polarization component). The different indices of refraction arise after imposing the condition of non-diagonal dielectric constant resulting in a nonlinear constitutive equation (Eq. 8.5 in Bohren and Huffman, 1998). Exact solutions for solid particles made of chiral molecules were found for the case of homogenous (Bohren, 1974) and layered spheres (Bohren, 1975).

Applequist (1977) provided a graphic explanation on how this physical interaction operates. When incident polarized light is modeled as a combination of two (right and left) circular polarized waves, each wave interacts with each atom by inducing a dipole (black arrows in Fig. 2). The strength and direction of each dipole is directly dependent on the rotation of the incident wave and the orientation of the molecule polarizability at that point. The total induced dipole, that is, the aggregated effect of all molecules' induced dipoles, will be different for each of the incident waves. A different total dipole for each wave results in a polarizability tensor that is not diagonal, and results in a non-linear change in the constitutive relationship between the displacement and electric field vectors (see Eq. 8.5 in Bohren and Huffman, 1998). The direct consequence of this effect is that two different indices of refraction need to be considered for each wave to obtain a solution in the Maxwell equations. The difference between the two results in the optical rotation effect.

Optical activity is observed in biological and non-biological compounds. However, non-biological OA materials have equal number of left and right molecules and generally have no net CP. Notably, biological chiral molecules are present in one type of handedness and in non-racemic mixtures which result in distinctive CP. Chiral molecules are present in biogenic aerosols and provide a path for their detection via optical methods, as it is discussed next.

In addition to pharmacology, optical studies of chiral molecules have been carried out in several fields for different applications. In molecular biology, optical polarimetry is a common technique because it is possible to non-destructively identify tissues, molecules, and cells. There have been significant developments in the use of optical activity to achieve this (Ghosh, 2011; Li et al., 2018; Purvinis et al., 2011; Qi and Elson, 2017; Westphal et al., 2016). Approaches were developed to measure and model the polarization signatures of biological particles in turbid media (Nafie, 1995; Sloot et al., 1989). Also, numerous works on instrumentation (Ahn et al., 2011; Bickel et al., 1976; Keller et al., 1985; Kunnen et al., 2015), theoretical and computational approaches (Autschbach, 2009; Ghosh, 2011; Ghosh et al., 2008; Videen, 1998; Wang et al., 2002; Wood et al., 2007), and reviews (de Boer and Milner, 2002; Savenkov, 2011; Tinoco and Williams, 1984) for applications in the medical sciences have been carried out. It is notable the amount of effort centered on the study of biological particles and tissues by means of measuring the full scattering matrix elements.

CP detection is also established in astronomy (Bailey et al., 1998; Meierhenrich et al., 2002; Rosenbush et al., 2007). The concept of chiral molecules has been invoked as a possible tracer of biomolecules in comets and extra-solar planets (Degtjarev and Kolokolova, 1992; Gledhill et al., 2007; Lucas Patty et al., 2018b; MacDermott, 1997). Excess of L- (or left) amino acids have been found in meteorites (Cronin and Pizzarello, 1997; Glavin and Dworkin, 2009). They showed that indeed homochirality exists outside the Earth in materials known to be fundamental in biological systems. The search for chiral signatures in meteorites remains an active area of research (Avnir, 2021; Glavin et al., 2020b, a) and is a candidate technique to detect biosignatures in future probes to Enceladus (MacKenzie et al., 2021; Neveu et al., 2020). Remote sensing of CP has been proposed as a technique for detection in comets and planets (Kolokolova et al., 2011). Measurements of CP from comets using spectropolarimeters have also been reported and chiral particles were suggested as a possible source of the observed CP (Rosenbush et al., 2007). Remote sensing of CP in space requires highly sensitive measurements (fractional polarizations well below 10^{-4}). However, modern developments in design and technology breakthroughs are making the detection of such signals possible (Craven-Jones et al., 2014; van Harten et al., 2011; Hough, 2011; Hough et al., 2006; Lucas Patty et al., 2017; Tyo et al., 2006).

These developments show that circular polarization is used to understand chiral particles in several diverse fields and is becoming increasingly feasible with technological advancement.

4 Alignment of particle as a source of circular polarization

As noted in Sect. 2, Eq. (2) is a commonly used form of the scattering matrix with some null off diagonal elements. The reasons invoked to set the coefficients $S_{41} = S_{42} = S_{14} = S_{24} = 0$ are the assumptions of randomly oriented particles and presence of equal number of mirror particles in the volume under observation. This results in a lower number of matrix coefficients to compute, thus achieving much faster results. Thus, modeled scattering by such aerosols with incident unpolarized light would result in no circular polarization in the first scattering event according to this formulation. It is the thesis of this work that some of these assumptions need to be reassessed considering additional evidence regarding aerosol morphology and their occurrence in the environment.

There are aerosol types known to be non-spherical at different stages while airborne. For example, pollen-shape inhomogeneities and dry marine aerosols result in detectable linear polarization (Haarig et al., 2019). Also freshly formed smoke contains abundant chains of coagulated soot particles (Chakrabarty et al., 2014; China et al., 2013; Girotto et al., 2018). A smoke cloud eventually ages, and a significant portion of particles become more spherical as they react with sunlight and water and organic vapors condense. Dust particles are also non-spherical (Gao and Anderson, 2001; Muñoz et al., 2001; Okada et al., 2001) and while different modeling approaches exist for the computation of their optical properties, they are expensive to run and only recently have satellite retrieval algorithms been incorporating non-spherical dust models (Gassó and Torres, 2016; Zhou et al., 2020). While the computation of matrix elements for single particles of these aerosol types will result in non-zero S_{34} and S_{43}, their impact in the ensemble of particles cancel out because the assumption of randomly oriented particles, which obscures the individual effects of particle shape (Mishchenko, 2014). However, in the case of oriented non-spherical particles such as dust aligned with an electromagnetic field (Fig. 3), the random particle orientation assumption is not fulfilled and the elements S_{41}, S_{42}, S_{14}, and S_{24} should be non-zero. In this case, the particle shape favors charge separation, and the resulting induced dipole in each particle aligns with the electrical field (Mallios et al., 2021). This concept has been applied in astronomy studies where the observations of linear and circular polarization in comets and interstellar dust could not be properly reproduced by models with spherical particles. Rather, non-spherical dust models were required to successfully reproduce the observations (Gledhill and McCall, 2000; Rogers and Martin, 1979; Schmidt, 1973; Vandenbroucke et al., 2021; Whitney and Wolff, 2002). Further, an interplanetary dust study by Kolokolova and Nagdimunov (2014) calculated the LP and CP in ensembles of spheroids oriented in a magnetic field and reported non-zero values for both. Notably they reported magnitudes of degree of CP comparable

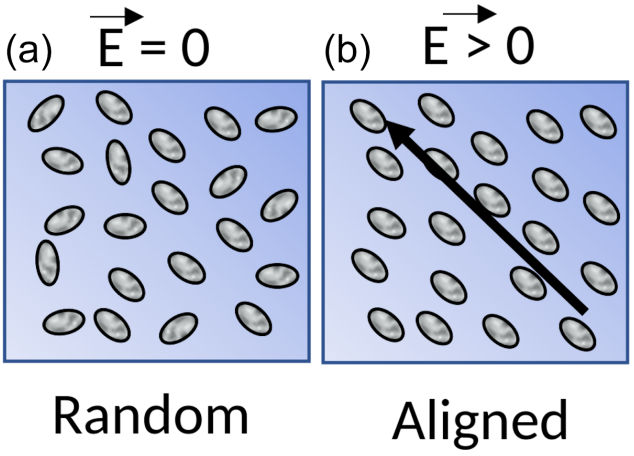

Figure 3. Dust particles in suspension are normally assumed as randomly distributed **(a)**. But in the presence of an electric field **(b)**, they tend to orient along (or precess around) the direction of the field.

to degree of LP for alignment angles between the major axis and the existing field between 0 and 90°.

With regards to Earth sciences applications, there is a growing body of evidence indicating the presence of electrical fields in volcanic ash (Harrison et al., 2010; Lane et al., 2011) and dust layers (Kamra, 1972; Nicoll et al., 2010; Ulanowski et al., 2007). Also, intense electrical fields are present in large fires so strong that they generate their own lighting (Dowdy et al., 2017; LaRoche and Lang, 2017). Further, smoke from fires have associated variability in the local atmospheric electrical field as it has been observed in Siberia (Ippolitov et al., 2013; Phalagov et al., 2009) . This variability was associated to changes in aerosol load, ambient moisture, and actinic flux (Nagorskiy et al., 2022). The presence of electrical fields and the fact that fresh smoke particles are non-spherical aggregates suggests the possibility of charge distribution within particles and possible alignment with the ambient electrical field.

There are additional interesting features to note. While it has been known that electrical fields are present during dust emission and play a role in the amount of dust lifted (Esposito et al., 2016; Kok and Renno, 2008; Zhang and Zhou, 2020), non-background electrical fields are also found in dust clouds at significant distance from the sources such as dust reaching Greece and the UK (Daskalopoulou et al., 2021; Harrison et al., 2018). These studies suggested triboelectrification (i.e., friction between particles) as mechanism for generation of an electric field within the cloud during transit.

The presence of an electric field may influence the natural sedimentation process of the particle and may provide an explanation for unexplained observations of very large particles found in dust clouds thousands of kilometers from the source (Denjean et al., 2016; Maring, 2003; Ryder et al., 2013). As suggested by Ulanowski et al. (2007), the electrical field can

impact the aerodynamics of large particles by counteracting gravitational sedimentation and cause a preferential orientation in non-spherical particles (Mallios et al., 2021; Toth III et al., 2020).

In summary, circular polarization has been observed originating in interstellar dust, and in this case only by assuming particle alignment in the presence of an electromagnetic field the optical properties can be modeled to match observations. Since electrical fields are present in dust clouds in the Earth's atmosphere, it may well be possible that these oriented particles scatter circular polarized light as well.

5 Observations of aerosol circular polarization

Most circular polarization studies in the Earth's environment have been limited to applications using active sensors or in the laboratory. Lidars with CP detection capabilities have been proposed for cloud phase and particle shape detection (Cao et al., 2009; Chaikovskaya, 2008; Donovan et al., 2015; Hu et al., 2003; Nicolet et al., 2012; Paschou et al., 2022; Tsekeri et al., 2021). Similarly, CP detection using lidars has been proposed to remotely detect bio-warfare agents (Pendleton and Rosen, 1998; Rosen, 1993), and to improve visibility and detection in underwater turbid environments (Gilbert and Pernicka, 1967; Lewis et al., 1999) and foggy atmospheres (van der Laan et al., 2018). These studies highlighted the fact that in high-concentration environments (AOD > 1), the propagation of circular polarization does not degrade with aerosol loading as quickly as linear polarization.

Recent developments show that CP can be measured with high precision using spectro-polarimetric techniques (Sparks et al., 2009b). Martin et al. (2010) measured the CP scattered by biogenic and dust aerosols and illustrated the difference in the matrix element S_{14} in those aerosols. The magnitude of particle CP (expressed as the ratio S_{14}/S_{11}) can vary significantly with values as high as 0.02 reported for particles in suspension or even higher for individual particles (Pan et al., 2022; Shapiro et al., 1990) or they can be as low as 10^{-5} (Sparks et al., 2009a). Figure 4 (Sparks et al., 2009b) shows measurements of CP transmission spectra in phytoplankton and a non-biogenic aerosol (dust). Figure 4b confirms earlier observations of lack of CP in dust and volcanic rocks reported first in Pospergelis (1969). The Sparks et al. (2009b) study demonstrated the clear contrast in CP when comparing biological with non-biological materials. As shown, the spectral CP is wavelength-dependent, with a dramatic sign reversal at roughly 680 nm (marked with a vertical dashed line). This is a phenomenon referred to as the Cotton effect and it is a known biogenic spectral signature (Barron, 2009).

The above-mentioned studies (Martin et al., 2016; Sparks et al., 2009a, b) and others (Lucas Patty et al., 2018a; Nouri et al., 2018) have used spectropolarimeters in laboratory settings with enough sensitivity ($< 10^{-4}$) to detect DCP signals from biogenic aerosols. These technologies not only have demonstrated that the full Stokes vector can be remotely measured with passive sensors but they are also amenable to be adapted in more portable forms (Rubin et al., 2019) or are already being built for aircraft deployments (Lucas Patty et al., 2021).

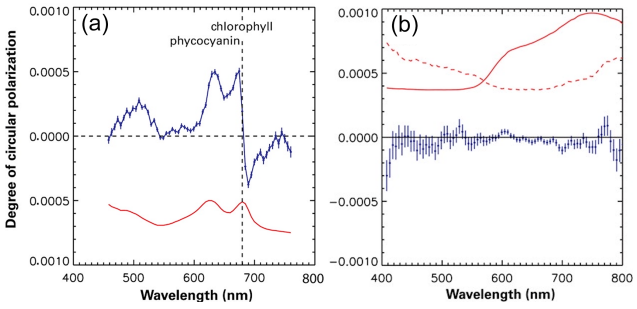

Figure 4. Non-zero and near zero transmission CP (solid blue line) spectra of a cyanobacteria **(a)** and from a control mineral **(b)**. The solid red line in **(a)** is a scaled version of the absorbance spectrum. Vertical dashed line points the reversal in sign in CP. Solid red in **(b)** shows the reflection spectrum of iron oxide, and the dashed red line shows the degree of linear polarization, both arbitrarily scaled (Sparks et al., 2009b).

There are very few reports of measurements of circular polarization specifically addressing atmospheric aerosols. Perhaps one of the most representative was made by Bickel et al. (1976) who reports a technique to measure all polarization states of light scattered by atmospheric aerosols. They showed several examples of non-zero circular polarization in pollen and bacterial spores as a function of scattering angle. Figure 5 shows an example of circular polarization scattered by two different spores illuminated with linearly-polarized light, as reported by Bickel and Stafford (1996). Because of these observations, Bohren and Huffman (1998) suggested (Sect. 13.8.5) the use of S_{34} measurements as a way to detect biological particles. Further, this is not the only non-zero element S_{4j} or S_{i4} of the scattering matrix. Laboratory measurements of CP of biological particles confirm that the element S_{14} is non-zero for individual (Lofftus et al., 1988; Pan et al., 2022) and ensembles of particles (Shapiro et al., 1990), although in the latter the magnitude tends to be lower than for single particles. This is an intriguing aspect that should be further explored as a non-zero S_{14} element implies that circular polarization should be present with incident unpolarized light such as sunlight. This can be easily realized by multiplying the incident sunlight vector ($I_{\text{sun}} = [I, 0, 0, 0]$) by Eq. (1).

Additional laboratory studies reported optical properties, including CP, of hydrosols (a.k.a. aerosol in aqueous environments) such as chloroplasts (Gregory and Raps, 1974) and dinoflagellates (Shapiro et al., 1990, 1991). These particles are also commonly found in the atmosphere and are considered biogenic marine aerosols. For the case of dinoflagel-

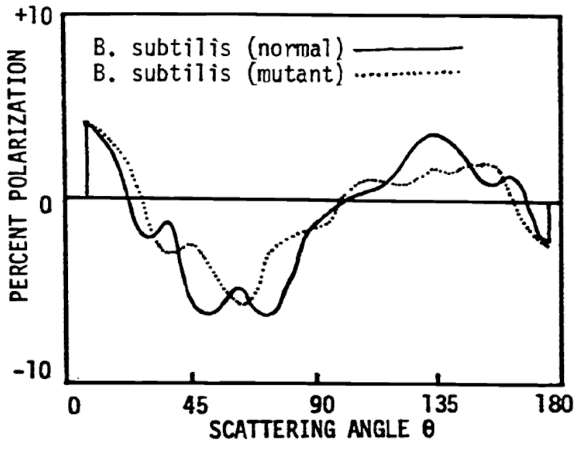

Figure 5. Spores are known biogenic aerosols and commonly found in the atmosphere, and as this example illustrates, they scatter circular polarized light. This figure shows the scattering matrix element measured for one type of spores and its mutant form for incident linearly polarized light. The variability of $S*_{34}$ (ratio of $(S_{14}+S_{34})/(S_{11}+S_{31})$) as a function of angle is displayed (Bickel and Stafford, 1996).

lates, Liu and Kattawar (2013) used a discrete dipole approximation code to simulate the helicoidal shape of the chromosome (a chiral structure) in the phytoplankton to calculate the 16 Mueller matrix elements. They found a non-zero S_{14} element in backscattering conditions consistent with previously reported observations. They suggested backscattering observations of S_{14} as possible method to detected dinoflagellates present in red tides. For atmospheric applications, it should be noted that hydrosols are ejected or are precursors of atmospheric biogenic organic aerosols (BOAs) in the marine environment, and they exhibit chiral signatures. For example, a number of studies reported (Kuznetsova et al., 2005; Wedyan and Preston, 2008) measurements of the chirality of amino acids in organic films of ejected marine aerosols.

With regards to reports of observed CP in atmospheric aerosols, the available evidence is limited because there are very few studies specifically focusing on the V Stokes parameter. For example, although polarized light has been proposed as a tool to improve visibility observations in the atmospheric marine boundary layer (Quinby-Hunt et al., 1997), the concept of using CP for the purposes of target detection has been overlooked. However, as we show, there is a reasonable amount of evidence that biogenic aerosols do contain chiral materials, and this suggests these aerosols should have distinctive CP signatures. In contrast, several investigations on the chiral nature of commonly found atmospheric aerosols have become available in the last decade. For example, naturally formed secondary organic aerosols (SOAs) have a distinct chiral structure in the Amazon forests (Ebben et al., 2011; Martinez et al., 2011) and in maritime pine forests (Staudt et al., 2019). The fact that aerosol gaseous precursors are chiral is important because the chirality of the gas remains when it forms or attaches to an aerosol as shown by Ebben et al. (2012). Enantiomeric monoterpenes (another biogenic gas emitted by plants, (Ganjitabar et al., 2018) and a precursor of SOA) have been measured in forests of South America and northern Europe (Song et al., 2014; Williams et al., 2007; Yassaa et al., 2001). Isoprene, another known aerosol precursor, is also produced in the marine environment by phytoplankton and is associated with the formation of BOAs in the atmosphere above (Colomb et al., 2008). It has been found in different enantiomer forms in ambient aerosols and used as a tracer to determine whether an aerosol is of primary or secondary origin (Noziere et al., 2011; Cash et al., 2016). Also, the chiral nature of a biogenic aerosol decays with aging through oxidation (Salma et al., 2010) suggesting that chirality detection may be used as a marker for aerosol aging.

The presence of left and right amino acids has been used for tracing the aerosol origin of marine aerosols and to determine their age in the Antarctic atmosphere (Barbaro et al., 2015; Kuznetsova et al., 2005). Also, circular dichroism has been observed in aerosol water extracts and atmospheric humic substances (HULIS) obtained from $PM_{2.5}$ µm samples in rural, urban, and in tropical environments, and has been suggested as a possible way to differentiate the aerosol between anthropogenic and natural formation processes (Salma et al., 2010). González et al. (2014) determined the distinctive chirality in BOAs to distinguish between aerosols of primary and secondary origin. Chiral behavior in aerosols has not only been reported over land but also in the marine environment (Yassaa et al., 2008). Further, glucose is one of the main components found in all biogenic organic aerosols (Samaké et al., 2019) and given that glucose is a chiral molecule and naturally present as one type of isomer (D-(+)-glucose), focusing efforts to detect CP from this molecule in BOA seems appropriate.

Perhaps one of the more compelling observations of aerosol's circular polarization in the Earth's atmosphere is reported by Petäjä et al. (2016). The BAECC (Biogenic Aerosols – Effects on Clouds and Climate) Campaign was carried out during spring and summer 2014 in the Finish arctic forest, and it focused on characterizing the role of biogenic aerosols in cloud formation. The aircraft deployed included in situ composition measurements and it operated near a ground-based high-spectral-resolution lidar (HSRL) lidar that specifically measured circular polarization (Robert Holtz, personal communication, 19 August 2019) as opposed to linear polarization, the more standard way to observe pollen with lidars (Sassen, 2008; Shang et al., 2022). The campaign included several examples of collocated surface lidar observations and aircraft overpasses at a time of the year where pollen and other biogenic aerosols are abundant. The resulting dataset is unique in that it contains remotely observed CP along with in situ confirmation of biogenic aerosols, known to contain chiral molecules. Figure 6 shows an example from this study where aircraft in situ in-

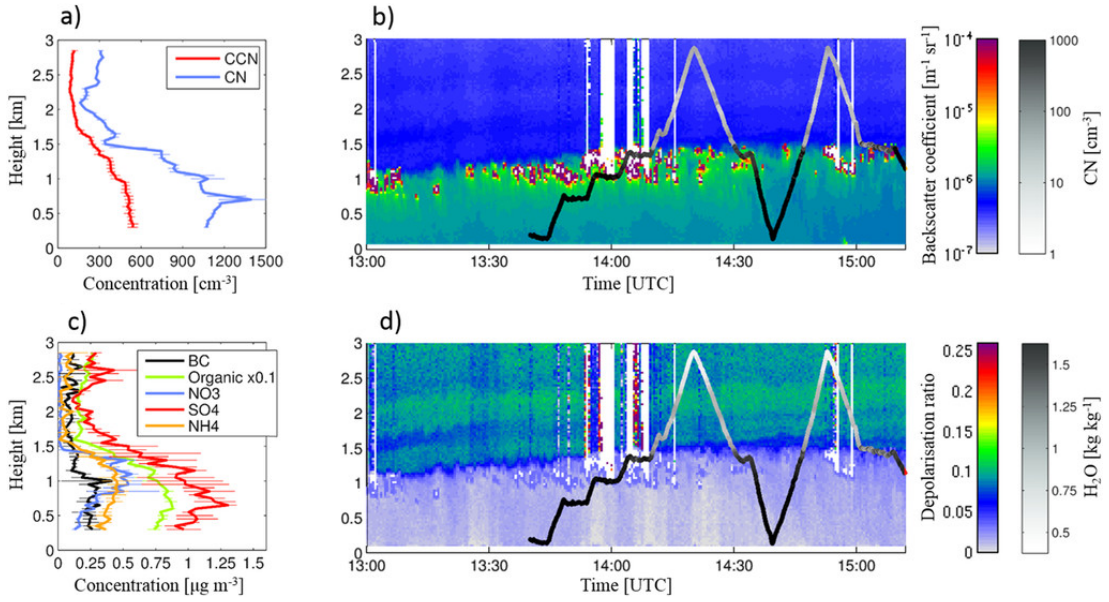

Figure 6. During springtime, forests are known to contain significant quantities of biogenic organic aerosols (such as pollen) and are good candidates for detection of circular polarization. Panel **(d)** shows near zero depolarization CP (which corresponds to high CP) above a forest in Finland where particle concentrations are rather high (profiles measured by aircraft, in panels **a** and **b**) and aerosol composition consistent with organic aerosols **(c)**. Panels **(b)** and **(d)** include airplane aerosol concentration and ambient water vapor (from Petäjä et al., 2016).

strumentation data and the corresponding lidar profile are displayed. The left column panels (a and c) show aircraft profiles of high CCN and aerosol concentrations in the boundary layer (panel a) and composition measurements demonstrating the high organic carbon content (green line in panel c) in the boundary layer, consistent with biogenic aerosols (also confirmed by Lee et al. (2018) in this campaign). Panel b shows the lidar profile (from surface) of backscattering with an in situ profile of aerosol concentration and both confirm the presence of high concentrations in the boundary layer. Panel d displays a profile of circular depolarization where a low value implies high circular polarization was observed. In this case, high CP values are reported in the boundary layer where the in situ data confirm the presence of biogenic aerosols. Petäjä et al. (2016) interprets the high CP as a manifestation of high LP expected if the particles are spherical which may be the case since ambient water content, and thus aerosol swelling by humidification was high. Although it is not explicitly mentioned, Petäjä et al. (2016) used an known correspondence between high CP with high LP as expressed by an equation derived by Mishchenko and Hovenier (1995) (MH95 for short). This is reasonable since there are not many lidar measurements of aerosol CP and the authors use this equation to relate the observed CP with the better-known and characterized lidar LP. This expression is frequently used in the lidar community to transform between lidar-derived backscatter LP and CP (Robert Holtz, personal communication, 19 August 2019). While the inference offered by Petäjä et al. (2016) is consistent with the state of knowledge of the time, an alternative interpretation is that CP is the result of the presence of chiral molecules in the biogenic aerosols which, as noted in previous sections, do exhibit CP.

Interestingly the distinctive CP found by lidar is in agreement with the theoretical modeling study by Kolokolova and Nagdimunov (2014) where optically active particles were shown to have non-zero CP and zero linear polarization in the backscattering direction. However, a controlled study (Cao et al., 2011) measuring the degree of LP and CP in pollen backscattering found that both scale with each other following the predictions of Mishchenko and Hovenier (1995). That study concluded there is no additional aerosol information by measuring both LP and CP. While the authors did not set out to seek for polarization signal in biogenic aerosols, there could be plausible reasons why no positive CP was observed. These include aging of the pollen (chirality disappears with aerosol senescence as shown by Salma et al., 2010 and in decaying leaves Lucas Patty et al., 2017), not enough representative samples, and lack of instrument sensitivity. This result should be confirmed as it appears to be the only one in the literature found measuring both atmospheric aerosol LP and CP simultaneously. While these two offer somewhat conflicting conclusions, both highlight that indeed biogenic aerosols do produce circular polarization. Clearly additional studies need to be carried out on the independence of information brought by the fourth Stokes term.

Overall, these measurements show that chirality detection is useful not only for aerosol type identification but also for

determination of particle creation mechanism and particle type. However, while these studies stress the fact that atmospheric aerosols do contain optically active components, most of the studies highlighted here were conducted with in situ instrumentation in field deployments or in controlled laboratory settings. To the extent of our research, we have found only one study (Petäjä et al., 2016) where remote sensing instrumentation in combination with in situ (essential to independently confirmed presence of biogenic aerosols) was utilized to detect circular polarization in aerosols.

6 Circular polarization propagation in the atmosphere

The study of circular polarization propagation has received significant attention outside the Earth sciences. For example, there is considerable amount of work in the field of astronomy to identify interstellar dust in the presence of magnetic fields (Sect. 3). In addition, there has been significant theoretical and modeling work towards understanding the propagation of CP in dense media such as tissues or dense biological liquids (Autschbach, 2009; Ghosh, 2011; Ghosh et al., 2008; Videen, 1998; Wang et al., 2002; Wood et al., 2007). This contrasts with the handful of theoretical works published on radiative transfer that considered oriented nonspherical particles or chiral particles in low-density medium such as an Earth-like atmosphere. Probably the only work on the development of the radiative transfer equations for chiral media in a planetary atmosphere were the studies by Kokhanovsky (1999, 2002). Specially, Kokhanovsky (1999) found the solution of the vector radiative transfer equation in the single scattering approximation, but no additional work has been published with this line of research. The design of a radiative transfer code that ingests chiral or non-symmetric oriented particles scattering matrix requires the treatment of a scattering matrix with two angles (scattering and inclination) as well as consideration of the effect of chiral or oriented particles on the extinction matrix, resulting in the dichroic extinction of the propagating light. To date, there are no algorithmic approaches available that consider these phenomena (Ping Yang, personal communication, 10 January 2022). However, such tools do exist for spherical homogenous particles, and it is with one of these that the top-of-the-atmosphere main features of aerosol CP are illustrated. The next section presents a modeling study with idealized conditions to simulate propagation of CP in an Earth-like atmosphere.

6.1 An application: CP from multiple scattering in an ideal atmosphere

Multiple scattering by an ensemble of particles can result in circular polarization (Kawata, 1978; Slonaker et al., 2005). Equation (4) shows the resulting fourth Stokes vector element (V) after two scattering events for incident unpolarized light onto an ensemble of randomly oriented particles with equal number of mirror symmetric particles (see Appendix A for derivation):

$$V_{\text{out}} = I_{\text{in}} s_{12} S_{34} \lceil \cos(2(\pi - m_2)) \cdot \sin(2(-M_1) + \sin(2(\pi - m_2)) \cdot \cos(2(-M_1)) \rceil, \quad (4)$$

where V_{out} and I_{in} are components of the outgoing and incident Stokes's vector, s_{12} and m_2 are scattering matrix elements and meridian angle (defined in Fig. A1) corresponding to the first scattering event, and S_{34} and M_1 are the same terms but for the second scattering event. In this case, the first interaction results in linear polarization which becomes the incident radiation for the second scattering event.

As an illustration on how the different components of the Stokes vector vary as a function of aerosol size distribution, composition, and concentration, radiative transfer computations of the top of the atmosphere (TOA) radiances at a fixed geometry for selected aerosol models are shown. The objective is to illustrate how the degree of linear and circular polarization compares with each other in ideal viewing conditions such as in the case of atmospheric aerosols over a dark surface.

The general model aerosol setup is for a hypothetical biogenic marine aerosol with a dark background surface. The aerosol models chosen for the simulations are generic in the sense they are consistent with marine aerosol models with bilognormal size distributions. The variability of composition and size is studied by considering two sets of simulations, one with a fixed bilognormal distribution and variable moderate absorption, and another with a variable fine mode fraction (FMF) of the total number of particles and fixed refractive index. The goal is to capture a reasonably wide optical range in aerosol size (as expressed by variable FMF) and different refractive indexes. Instead of explicitly considering parameterizations as a function of wind and ambient relative humidity (both known to impact atmospheric radiances through changes in size and index of refraction), we choose a more practical approach by prescribing the FMF and refractive index with a wide range of values expected to be present in marine biogenic aerosols. Parameters selected here were chosen to be consistent and within ranges of the marine aerosol models reported in Sayer et al. (2012). Thus, the simulated case assumes the following conditions: aerosols with very low to high concentrations, homogenously vertical distributed from the surface to 1 km, and bi-lognormal size distributions with varying coarse mode concentrations. The details are as follows. The size distribution is made of two lognormal distributions with a variable fine mode fraction ($0 < \text{FMF} < 1$) defined as in $\text{d}V/\text{dlog}R = \text{FMF} \cdot \text{d}V\text{fine}/\text{dlog}R + (1\text{-FMF})\,\text{d}V\text{coarse}/\text{dlog}R$ with $R_{\text{vol,fine}} = 0.1165\,\text{um}$, $\text{STD}_{\text{fine}} = 1.4813$, $R_{\text{vol,coarse}} = 2.8329\,\text{um}$, $\text{STD}_{\text{coarse}} = 1.9078$ (based on Dubovik et al., 2000, JAS). With respect to the refractive index, three composition models are considered. One model (labeled "low") has $n = 1.50–i1.0 \times 10^{-4}$ and the other

model ("high") $1.50–i.0 \times 10^{-3}$ for all wavelengths in both models. A third model ("mixed") has a constant real part with spectrally dependent imaginary refractive index and different composition in each mode: fine mode $= 1.45+i5.0 \times 10^{-3}$ to 2.0×10^{-4} and coarse mode $= 1.50 + i1.0 \times 10^{-4}$ to 1.0×10^{-6}. The spectral range chosen includes an assortment of wavelengths from the near-UV to near-IR (in um): 0.3400, 0.3880, 0.4700, 0.7650, 2.210. The particle shape is assumed to be spherical. The atmospheric column only contains pure air (i.e., no trace gases) with a surface pressure set at 1013 mbar, surface reflectance is set to zero, sun zenith angle is 40°with variable azimuth, and view angles set at regular spaces. Aerosol loadings range from AOD (0.55 um) from 0 to 1.2. The only radiative processes considered are aerosol and Rayleigh scattering. The solar constant is set to unity. The radiative transfer model is a Gauss–Seidel vector code ("the Arizona Code") created by Herman et al. (1995) and is frequently used in near-UV satellite applications (Herman et al., 2001; Herman and Celarier, 1997). The code outputs the four Stokes components of the upwelling radiance (I, Q, U, and V) and then the degree of linear polarization (DLP $=$ SQRT$(Q^2 + U^2)/I$) and circular polarization (DCP $= |V|)/I$) are computed.

6.2 Results

Figure 7 provides an example of these simulations. Three panels show the total intensity, DLP, and DCP as a function of aerosol loading (AOD at 0.551 µm) at five representative wavelengths for an aerosol model dominated by fine mode particles (FMF $= 0.98$). Before pointing out features to note, it is useful to reiterate a few concepts here. The Rayleigh molecular scattering cross section model is strongly dependent on the inverse fourth power of the wavelength, and it has a minimal influence on scattering in high wavelengths (roughly $\lambda > 0.6$ µm). Thus, the interplay of aerosol and molecular scattering will be strongly dependent on the region of the spectrum. Also, multiple scattering is strongly dependent on particle concentration and its impact on observed parameters will be more apparent at higher AODs.

For no aerosols (AOD $= 0$), no circular polarization is present since molecular scattering only results in linear polarization. The intensity (left panel) remains constant at low AODs (AOD < 0.1) and then increasing with aerosol loading mostly in the visible and near-UV channels because most of the scattering is occurring in the fine mode which is the dominant aerosol concentration in this simulation (the impact of the presence of a variable coarse mode is explored later).

In considering DLP (center panel), the effect of multiple scattering is a strong function of aerosol loading and wavelength. Below 0.5 µm, molecular scattering provides a background of linearly polarized light incident on the aerosol. This effect is most apparent at these wavelengths even in the low AOD range. As aerosol concentration increases, the number of scattering events between Rayleigh and aerosols also increase. Linear polarization is an expression of the prevalence of single scattering aerosol events which increases with loading. However, at a certain loading level, the number of second scattering events starts to be dominant and linear polarization degrades. This is particularly apparent in the shortest three wavelengths where multiple scattering is dominant at all aerosol loadings. At the higher wavelengths (0.76 and 2.2 µm), the Rayleigh contribution is minimal, and the only linear polarization observed is originating from primary aerosol scattering. Aerosol-to-aerosol scattering interactions are prevalent at these wavelengths and aerosol concentration becomes the dominant effect. In the case of the 0.76 µm wavelength, a second scattering event starts to be dominant at AOD ~ 0.4 and the contribution of LP to the observed signal is dampened. At 2.2 µm, single scattering dominates through the AOD range considered.

The degree of circular polarization (DCP) is shown in the right panel of Fig. 7. There are several features to note. First, with no aerosols (AOD $= 0$), there is no circular polarization present as expected. Second, while the absolute magnitudes of DCP are low compared to DLP, the change with loading is significant. Third, there is a strong wavelength dependency in the DCP magnitude. There is no DCP at the 2.21 µm wavelength and it is highest at the VIS and NIR wavelengths (0.47 and 0.76 µm) and intermediate for the near-UV wavelengths. This suggests an interplay between the presence of Rayleigh effect in the different spectral ranges. At 2.21 µm, scattering is only originating from aerosols and possibly there are not enough scattering events to produce meaningful LP and subsequent second scattering events to generate CP. At the lowest wavelength (0.34 µm, blue line), LP from Rayleigh scattering is the dominant initial source of polarization, and the addition of aerosols has an immediate multiple scattering effect in diminishing the DLP (center panel) and resulting in more second scattering events. The resulting increase in CP with loading appears to be limited (it flattens around AOD $= 0.5$). The variability in LP and CP for the intermediate wavelengths (0.380, 0.47, and 0.765 µm) is more difficult to interpret but it is clear it results from the interplay of Rayleigh scattering-dependence on wavelength and aerosol concentration available enabling different orders of scattering.

The magnitude of both DLP and DCP as a function of loading are strongly dependent on the viewing geometry whereas it is less so for total intensity. For example, Fig. 8 shows intensity, DLP, and DCP for the same aerosol model and conditions of Fig. 7 but for a different scattering angle. In comparison with Fig. 7, the magnitude of the intensity increases slightly, and it does not vary significantly with a change of geometry. However, DLP is reduced by a factor of 3–4 whereas DCP is augmented by a factor of 2–3. Also, the shape of the DLP curves appear dampened in Fig. 8 whereas the slope of the DCP curves is markedly steeper. Finally, at both geometries the same range of wavelengths (0.38 and 0.47 µm) had the highest CP magnitudes. The contrast in po-

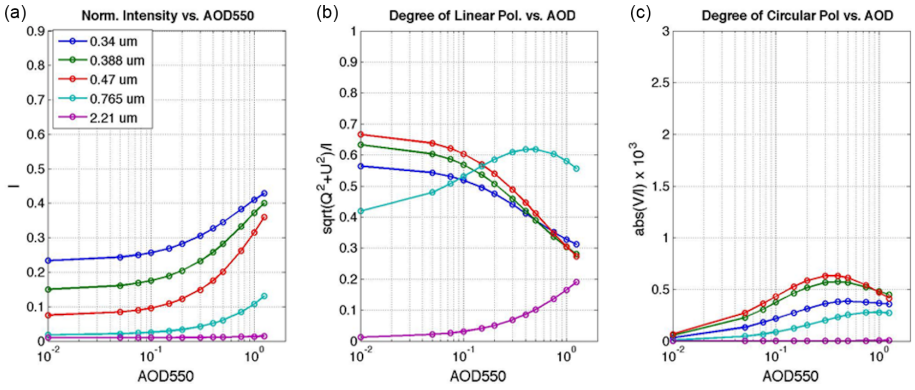

Figure 7. Top of the atmosphere normalized radiance **(a)**, and degree of linear **(b)** and circular (**c**, multiplied by 10^3) polarization as a function of aerosol optical depth (AOD) at 550 um for selected near-UV to near-IR wavelengths at scattering angle 103.2°(SZA = 40, VZA = 40, RelAzim = 30). This is the mixed aerosol model with high concentration of particles in the fine mode and a minimal contribution of the coarse mode (FMF = 0.98).

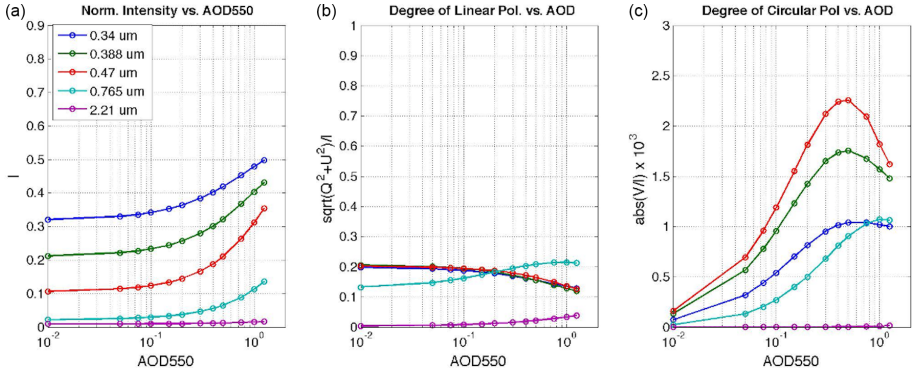

Figure 8. Top of the atmosphere normalized radiance **(a)**, and degree of linear **(b)** and circular (**c**, multiplied by 10^3) polarization as a function of aerosol optical depth (AOD) at 550 um for same aerosol properties as Fig. 7 but with a different scattering angle 142.5°(SZA = 40, VZA = 40, RelAzim = 120).

larization features between Figs. 7 and 8 illustrates the importance of viewing geometry in polarimetric observations.

The role of the dominance of coarse and fine mode particles and composition are evaluated next. These simulations were carried out with a goal to explore if compositional differences (expressed optically through different refractive indexes and size distribution) arise in the Stokes vector components. This analysis focuses on low aerosol loading ranges ($\tau_{aer} = 0$ to 0.2) because this is the range of concentrations most globally prevalent (Anderson et al., 2013; Knobelspiesse et al., 2012; Levy et al., 2015; Remer et al., 2008) and for which current approaches have the least sensitivity to aerosol type. In all cases, the pure Rayleigh atmosphere ($\tau_{aer} = 0.0$) is included as a reference point.

These simulations are shown in Fig. 9 at two representative wavelengths. The intensity plots (panels in the first column) show an expected behavior. In the near UV, molecular scattering is dominant and the changes in aerosol loading and fine mode contribution add minor increases compared to the baseline. Also, no differences are noted due to aerosol composition (the three lines are very close to each other). At 0.865 µm, the Rayleigh contribution can be ignored, and given that the surface is dark, the signal originates only from aerosols. Note the significant difference in magnitude and the clear increase of radiance as a function of aerosol concentration as expected in the single scattering regime. Both panels illustrate the lack of aerosol identifying information in intensity-only observations at these aerosol loading ranges.

The linear (center column panels) and circular (right) polarization features are discussed next. DLP has a more noticeable dependency on the contribution of FMF. For the near-UV, multiple scattering is dominant resulting in immediate decrease of linear polarization as function of FMF and loading because both tend to increase the number of scattering events. This is not the case at 0.865 µm where linear polarization increases with both AOD and FMF. Note the contrast in magnitude changes in both wavelengths. In practical terms, the relative changes in DLP magnitude at 0.380 µm is not significant as function of loading, composition, and FMF. But at 0.865 µm, there is notable change with AOD and FMF

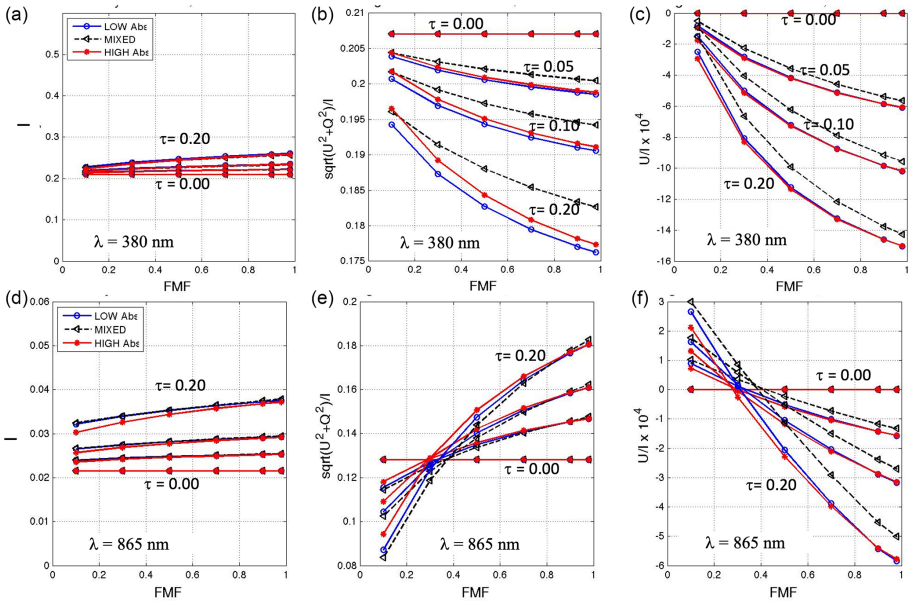

Figure 9. Intensity **(a, d)**, degree of linear polarization **(b, e)**, and normalized circular polarization **(c, f)** as a function of fine mode fraction (FMF) for three aerosol models with different imaginary refractive index: model with low and high spectrally invariant absorption and a case with spectrally dependent absorption (mixed). See Sect. 6.1 for details. Angles are the same as in Fig. 8.

but negligible for composition. For circular polarization, it is notable the large change in absolute and relative magnitude at both wavelengths as function of FMF and it is more pronounced at higher loadings. However, the sensitivity to composition is not particularly noticeable at these loadings.

Overall, these plots suggest there is a sensitivity to differences between coarse and fine mode-dominated aerosols in both linear and circular polarization. In terms of absolute and relative magnitude change and considering both wavelengths, circular polarization is more sensitive to modal variability. More importantly, both linear and circular polarization demonstrate a sensitivity to aerosol properties that are not present in the intensity-only plots.

While not comprehensive, these simulations illustrate the patterns in circular polarization for representative aerosol loadings, composition, and size distributions. They demonstrate that CP can be highly variable and has variable magnitude as a function of aerosol properties in conditions where LP does not change much (Figs. 8 and 9). It demonstrates that CP may contain aerosol information in instances when LP loses its sensitivity to aerosol properties as aerosol optical depth increases. A more formal way to determine the unique value of CP contained in observed polarized radiances would require an information content assessment that incorporates all observations simultaneously and accounts for expectations of model and measurement uncertainty. Successful studies for this application have used the Bayesian locally linear approximation method of Rodgers (Hasekamp and Landgraf, 2007), or a full Bayesian approach (Knobelspiesse et al., 2021).

7 Summary and recommendations

It has been more than 40 yr since polarimetric sensors were deployed to study planetary atmospheres: Pioneer 10 and 11 were sent to Jupiter in 1972 and 1973, respectively, and Pioneer 12 was sent to Venus in 1978 (Murdin, 2001; NASA, 20211). All three missions carried out the same imaging polarimeter (Gehrels et al., 1980). Their observations resulted in several novel computations and theoretical studies focused on full polarization in cloudy atmospheres. These studies suggested that while circular polarization (CP) originating from clouds was observed, no significant additional information appears to be gained by measuring the fourth Stokes coefficient. These conclusions, combined with the low magnitude of observed circular polarization compared to linear polarization and total intensity resulted in little subsequent interest in the development of full polarization sensors for remote sensing applications and related theoretical understanding.

Five decades later, technological advances now enable a wider use of circular polarization in several applications including remote detection of aerosols. Additionally, there is new knowledge of sources of CP in the atmosphere. It is now reasonable then to reassess the advantages of carrying out full polarization remote sensing of atmospheric aerosols. The purpose of this overview is to provide a summary of these recent developments. This report is concerned with the science motivations regarding aerosol properties and points out features that are likely (or already known) to produce circular polarization.

Three aerosol physical processes are explored as a source of aerosol circular polarization in the atmosphere:

1. Optical activity in biogenic aerosols (Sects. 3 and 5)
2. Alignment of non-spherical particles such as dust, volcanic ash, and smoke (Sect. 4)
3. Multiple scattering effects of aerosols (Sect. 6).

Observable CP in biogenic particles originates from molecules such as amino acids and proteins, both known to be chiral molecules with specific optical features and suggest a pathway to uniquely differentiate biogenic aerosols from non-biological aerosols. The presence of atmospheric electrical fields within clouds of non-spherical aerosols results in an alignment of particles and may provide asymmetries in the scattering process that may result in CP. While the presence of strong electrical fields in dust, volcanic ash, and smoke has been observed, circularly scattered light resulting from incidence of (unpolarized) sunlight remains to be observed. Finally, CP can arise because of multiple scattering processes in any group of particles.

The latter effect is further explored by carrying radiative transfer simulations for a typical set of aerosol models at different viewing geometries, wavelength, and aerosol loadings in idealized conditions (dark surface, no trace gases, and no clouds, only in a molecular atmosphere). The total intensity and the degrees of linear and circular polarization are compared against each other and features and differences among the three are highlighted. CP variability is noted in scenarios where total intensity and linear polarization do not appear to be as sensitive as a function of angle, loading, and spectral range. CP does degrade as a function of aerosol concentration, but not as much as linear polarization does. This may provide a pathway by which CP and LP can be used in combination to extract different aerosol information depending on the aerosol loading. As is common in polarization, CP is highly sensitive to viewing geometry and additional studies remain to be done to explore this aspect in relation to satellite observing geometries.

The above simulations are meant to provide limited illustration and extrapolation to more realistic settings need to be considered. Clearly there are important challenges to be sorted out in a realistic atmospheric setting. Observation of circular polarization requires precise and accurate measurements where instrument sensitivity and additional sources of instrumental noise need to be properly characterized. Moreover, there are additional (non-aerosol) sources of CP in the atmosphere that need to be considered and compared to those arising from the particles of interest. For example, circular polarization is contained in the incident solar radiation at the Earth's top of the atmosphere (DCP $\sim 10^{-6}$) (Kemp et al., 1987). Also circular polarization is expected to arise from the surface such as vegetation (Van Eeckhout et al., 2019; Lucas Patty et al., 2019a) . However, there have been no attempts to simulate scenarios with all these elements in place in a radiative transfer model and establish the different contributions to the top of atmosphere polarized radiances. Perhaps the closest to these scenarios are several studies in object detection in foggy or very turbid (including underwater) environments in the context of military applications. In general, these studies are interested in horizontal transmissivity of spectro-polarimetric signals and they do highlight the persistence of CP compared to LP (van der Laan et al., 2018; Zeng et al., 2018, 2019, 2020). However, none of these studies considered incident of unpolarized light or background conditions such as those in the atmospheric remote sensing setting.

This is the first work to summarize circular polarization in atmospheric aerosols. It gathers evidence from different disciplines (molecular biology, stereochemistry, astronomy, and astrobiology) where aerosol CP is present, and it discusses the possibilities of carrying out similar observations in atmospheric aerosols. Specifically, it offers a possibility by which atmospheric aerosols can be detected remotely and may provide a new tool to complement existing techniques of aerosol composition identification.

Appendix A

Derivation of the fourth Stokes vector component in the case of two scattering events for an aerosol particle with the following scattering matrix is as follows:

$$S(\Theta) = \begin{bmatrix} S_{11} & S_{12} & 0 & 0 \\ S_{12} & S_{22} & 0 & 0 \\ 0 & 0 & S_{33} & S_{34} \\ 0 & 0 & -S_{34} & S_{44} \end{bmatrix},$$

where the dependence on the scattering angle Θ (a function of the incident and viewing zenith (μ, μ') and azimuth angles (ϕ, ϕ')) in S_{ij} is assumed and omitted for simplicity in Eqs. (A2) and (A3). The transformation of coordinates (Chandrasekhar, 1960) to the local meridian planes is (as defined in Fig. A1)

$$L(\Theta) = R(\pi - m_2) \cdot S(\Theta) \cdot R(-m_1), \tag{A1}$$

where R is the rotation matrix transforming from the particle centered frame of reference to the observer's frame of reference and is defined as

$$R(\psi) = \begin{bmatrix} 1 & 0 & 0 & 0 \\ 0 & \cos(2\psi) & \sin(2\psi) & 0 \\ 0 & -\sin(2\psi) & \cos(2\psi) & 0 \\ 0 & 0 & 0 & 1 \end{bmatrix},$$

with $\psi\pi - m_2$ or $= -m_1$, and m_1 and m_2 are the angles between the meridian planes containing incident and scattered vectors and the scattering plane (Fig. A1), respectively.

For incident unpolarized light (I_{in} [1,0,0,0]), the outgoing scattered radiation after the first scattering event can be ex-

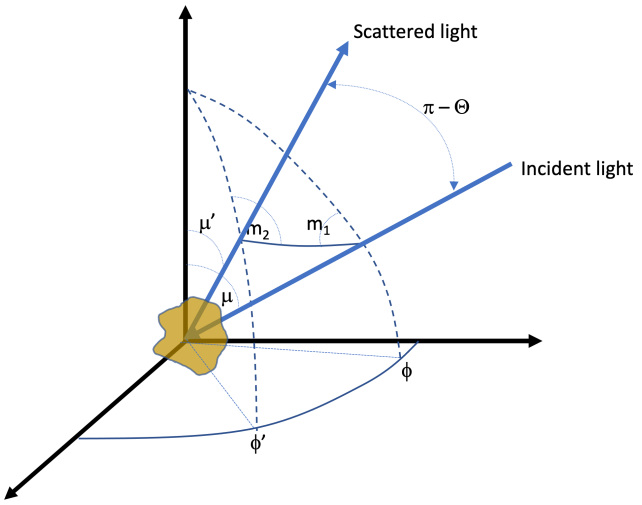

Figure A1. Angle definitions in a frame of reference centered in the scattering object: μ and φ (μ', φ') are the zenith and azimuth for the incident (scattered) light, Θ is the scattering angle defined by the plane that contains the incident and scattered light vectors, and m_1 and m_2 are the angles between meridian planes and the scattering plane.

pressed as (after Eq. 1 in Sect. 2)

$$\begin{bmatrix} I_{\text{in}}S_{11} \\ I_{\text{in}}S_{12}\cos(2(\pi - m_2)) \\ -I_{\text{in}}S_{12}\sin(2(\pi - m_2)) \\ 0 \end{bmatrix}. \tag{A2}$$

The resulting vector after the first interaction has linear components that depends on the orientation of the reference planes, and it has no circular polarization ($V_{\text{out}} = 0$). If there is a second scattering event, the above vector (Eq. A2) is the incident light onto the second particle and a similar multiplication of matrixes (Eq. A1) occurs resulting in Eq. (A3),

$$V_{\text{out}} = I_{\text{in}}s_{12}S_{34}\left[\cos(2(\pi - m_2)) \cdot \sin(2(-M_1)) + \sin(2(\pi - m_2)) \cdot \cos(2(-M_1))\right], \tag{A3}$$

where the upper-case letters refer to the second scattering event and the lower case to the first event.

Data availability. The data from the model simulations and the implemented model codes are available from the authors upon request.

Author contributions. SG carried out literature gathering and review, performed the simulations, carried out the analysis, created the figures, and wrote the paper. KDK reviewed several versions of the paper, and provided several key suggestions and background material.

Competing interests. The contact author has declared that none of the authors has any competing interests.

Disclaimer. Publisher's note: Copernicus Publications remains neutral with regard to jurisdictional claims in published maps and institutional affiliations.

Acknowledgements. The work represents the culmination of an idea that originated in 2009 during NASA's working groups to develop the scientific objectives of the ACE mission (later evolved into current PACE and ATMOS missions). Thanks to program managers Hal Maring and Paula Botempi for their initial funding. The stimulating conversations through the intervening years with Bill Sparks, Robert Spurr, Craig Bohren, and Ludmilla Kolokova are also acknowledged as seminal to this work. Bill Sparks and Noah Rubin are thanked for the comments of early versions of the paper. Finally, Santiago Gassó is deeply thankful to Kerry Meyer (NASA/GSFC) who provided the funding for the compilation and completion of the work shown herein.

Financial support. This study was partially funded by the NASA Earth Science Technology Office via the Instrument Incubator Program (WBS: grant no. 478643.02.12.02.27).

Review statement. This paper was edited by Stelios Kazadzis and reviewed by three anonymous referees.

References

Ahn, C., Torres, O., and Jethva, H.: Assessment of OMI near-UV aerosol optical depth over land, J. Geophys. Res.-Atmos., 119, 2457–2473, https://doi.org/10.1002/2013JD020188, 2014.

Ahn, Y.-C., Chung, J., Wilder-Smith, P., and Chen, Z.: Multimodality approach to optical early detection and mapping of oral neoplasia, J. Biomed. Opt., 16, 076007, https://doi.org/10.1117/1.3595850, 2011.

Alsante, A. N., Thornton, D. C. O., and Brooks, S. D.: Ocean Aerobiology, Front. Microbiol., 12, 3143, https://doi.org/10.3389/fmicb.2021.764178, 2021.

Anderson, J. C., Wang, J., Zeng, J., Leptoukh, G., Petrenko, M., Ichoku, C., and Hu, C.: Long-term statistical assessment of Aqua-MODIS aerosol optical depth over coastal regions: bias characteristics and uncertainty sources, Tellus B Chem. Phys. Meteorol., 65, 20805, https://doi.org/10.3402/tellusb.v65i0.20805, 2013.

Applequist, J.: An Atom Dipole Interaction Model for Molecular Optical Properties, Acc. Chem. Res., 10, 79–85, https://doi.org/10.1021/ar50111a002, 1977.

Applequist, J.: Optical Activity: Biot's Bequest, Am. Sci., 75, 58–68, 1987.

Asano, S.: Light scattering properties of spheroidal particles, Appl. Opt., 18, 712, https://doi.org/10.1364/AO.18.000712, 1979.

Asano, S. and Sato, M.: Light scattering by randomly oriented spheroidal particles, Appl. Opt., 19, 962, https://doi.org/10.1364/AO.19.000962, 1980.

Autschbach, J.: Computing chiroptical properties with first-principles theoretical methods: Background and illustrative examples, Chirality, 21, E116–E152, https://doi.org/10.1002/chir.20789, 2009.

Avnir, D.: Critical review of chirality indicators of extraterrestrial life, New Astron. Rev., 92, 101596, https://doi.org/10.1016/j.newar.2020.101596, 2021.

Bailey, J., Chrysostomou, A., Hough, J. H., Gledhill, T. M., McCall, A., Clark, S., Ménard, F., and Tamura, M.: Circular Polarization in Star- Formation Regions: Implications for Biomolecular Homochirality, Science, 80, 672–674, https://doi.org/10.1126/science.281.5377.672, 1998.

Barbaro, E., Zangrando, R., Vecchiato, M., Piazza, R., Cairns, W. R. L., Capodaglio, G., Barbante, C., and Gambaro, A.: Free amino acids in Antarctic aerosol: potential markers for the evolution and fate of marine aerosol, Atmos. Chem. Phys., 15, 5457–5469, https://doi.org/10.5194/acp-15-5457-2015, 2015.

Barron, L. D.: Molecular Light Scattering and Optical Activity, 2nd Edn., Cambridge, Cambridge University Press, https://doi.org/10.1017/CBO9780511535468, 2004.

Bellcross, A., Bé, A. G., Geiger, F. M., and Thomson, R. J.: Molecular Chirality and Cloud Activation Potentials of Dimeric α-Pinene Oxidation Products, J. Am. Chem. Soc., 143, 16653–16662, https://doi.org/10.1021/jacs.1c07509, 2021.

Bian, H., Chin, M., Hauglustaine, D. A., Schulz, M., Myhre, G., Bauer, S. E., Lund, M. T., Karydis, V. A., Kucsera, T. L., Pan, X., Pozzer, A., Skeie, R. B., Steenrod, S. D., Sudo, K., Tsigaridis, K., Tsimpidi, A. P., and Tsyro, S. G.: Investigation of global particulate nitrate from the AeroCom phase III experiment, Atmos. Chem. Phys., 17, 12911–12940, https://doi.org/10.5194/acp-17-12911-2017, 2017.

Bickel, W. S. and Stafford, M. E.: Polarized scattered light as a probe for structure and change in bioparticles, in: Ultrasensitive Biochemical Diagnostics, vol. 2680, edited by: Cohn, G. E., Soper, S. A., and Chen, C. H. W., 4–15, SPIE, 1996.

Bickel, W. S., Davidson, J. F., Huffman, D. R., and Kilkson, R.: Application of polarization effects in light scattering: a new biophysical tool, P. Natl. Acad. Sci. USA, 73, 486–490, https://doi.org/10.1073/pnas.73.2.486, 1976.

Binkowski, F. S. and Roselle, S. J.: Models-3 Community Multiscale Air Quality (CMAQ) model aerosol component 1. Model description, J. Geophys. Res.-Atmos., 108, 4183, https://doi.org/10.1029/2001JD001409, 2003.

Bohren, C. F.: Light scattering by an optically active sphere, Chem. Phys. Lett., 29, 458–462, https://doi.org/10.1016/0009-2614(74)85144-4, 1974.

Bohren, C. F.: Scattering of electromagnetic waves by an optically active spherical shell, The J. Chem. Phys., 62, 1566, https://doi.org/10.1063/1.430622, 1975.

Bohren, C. F. and Huffman, D. R.: Absorption and Scattering of Light by Small Particles, 1st Edn., Wiley-VCH Verlag GmbH, Weinheim, Germany, 1998.

Born, M.: Herbert Herkner, Die Naturwissenschaften, 6, 179–180, https://doi.org/10.1007/BF01491442, 1918.

Cao, X., Roy, G., Roy, N., and Bernier, R.: Comparison of the relationships between lidar integrated backscattered light and accumulated depolarization ratios for linear and circular polarization for water droplets, fog oil, and dust, Appl. Opt., 48, 4130, https://doi.org/10.1364/AO.48.004130, 2009.

Cao, X., Roy, G. A., Cao, X., and Bernier, R.: On linear and circular depolarization LIDAR signatures in remote sensing of bioaerosols: experimental validation of the Mueller matrix for randomly oriented particles, Opt. Eng., 50, 1–11, https://doi.org/10.1117/1.3657505, 2011.

Cash, J. M., Heal, M. R., Langford, B., and Drewer, J.: A review of stereochemical implications in the generation of secondary organic aerosol from isoprene oxidation, Environ. Sci. Process. Impacts, 18, 1369–1380, https://doi.org/10.1039/C6EM00354K, 2016.

Chaikovskaya, L. I.: Remote sensing of clouds using linearly and circularly polarized laser beams: techniques to compute signal polarization, in: Light Scattering Reviews 3, 191–228, Springer Berlin Heidelberg, Berlin, Heidelberg, 2008.

Chakrabarty, R. K., Beres, N. D., Moosmüller, H., China, S., Mazzoleni, C., Dubey, M. K., Liu, L., and Mishchenko, M. I.: Soot superaggregates from flaming wildfires and their direct radiative forcing, Sci. Rep., 4, 5508, https://doi.org/10.1038/srep05508, 2014.

Chandrasekhar, S.: Radiative Transfer, Dover Publications In, New York, 1960.

China, S., Mazzoleni, C., Gorkowski, K., Aiken, A. C., and Dubey, M. K.: Morphology and mixing state of individual freshly emitted wildfire carbonaceous particles, Nat. Commun., 4, 2122, https://doi.org/10.1038/ncomms3122, 2013.

Coffeen, D. L.: Polarization and scattering characteristics in the atmospheres of earth, venus and jupiter, J. Opt. Soc. Am., 69, 1051, https://doi.org/10.1364/JOSA.69.001051, 1979.

Colarco, P., da Silva, A., Chin, M., and Diehl, T.: Online simulations of global aerosol distributions in the NASA GEOS-4 model and comparisons to satellite and ground-based aerosol optical depth, J. Geophys. Res., 115, D14207, https://doi.org/10.1029/2009JD012820, 2010.

Colomb, A., Yassaa, N., Williams, J., Peeken, I., and Lochte, K.: Screening volatile organic compounds (VOCs) emissions from five marine phytoplankton species by head space gas chromatography/mass spectrometry (HS-GC/MS), J. Environ. Monit., 10, 325–330, https://doi.org/10.1039/b715312k, 2008.

Craven-Jones, J., Harrington, D., Tyo, J. S., Escuti, M., Fineschi, S., Mawet, D., Riedi, J., Snik, F., and De Martino, A.: An overview of polarimetric sensing techniques and technology with applications to different research fields, in: Polarization: Measurement, Analysis, and Remote Sensing XI, vol. 9099, p. 90990B., 2014.

Cronin, J. R. and Pizzarello, S.: Enantiomeric Excesses in Meteoritic Amino Acids, Science, 80, 951–955, https://doi.org/10.1126/science.275.5302.951, 1997.

Daskalopoulou, V., Mallios, S. A., Ulanowski, Z., Hloupis, G., Gialitaki, A., Tsikoudi, I., Tassis, K., and Amiridis, V.: The electrical activity of Saharan dust as perceived from surface electric field observations, Atmos. Chem. Phys., 21, 927–949, https://doi.org/10.5194/acp-21-927-2021, 2021.

de Boer, J. F. and Milner, T. E.: Review of polarization sensitive optical coherence tomography and Stokes vector determination, J. Biomed. Opt., 7, 359, https://doi.org/10.1117/1.1483879, 2002.

Degtjarev, V. S. and Kolokolova, L.: Possible application of circular polarization for remote sensing of cosmic bodies, Earth, Moon

Planets, 57, 213–223, https://doi.org/10.1007/BF00057992, 1992.

Denjean, C., Cassola, F., Mazzino, A., Triquet, S., Chevaillier, S., Grand, N., Bourrianne, T., Momboisse, G., Sellegri, K., Schwarzenbock, A., Freney, E., Mallet, M., and Formenti, P.: Size distribution and optical properties of mineral dust aerosols transported in the western Mediterranean, Atmos. Chem. Phys., 16, 1081–1104, https://doi.org/10.5194/acp-16-1081-2016, 2016.

Després, V., Huffman, J. A., Burrows, S. M., Hoose, C., Safatov, A., Buryak, G., Fröhlich-Nowoisky, J., Elbert, W., Andreae, M., Pöschl, U., and Jaenicke, R.: Primary biological aerosol particles in the atmosphere: a review, Tellus B Chem. Phys. Meteorol., 64, 15598, https://doi.org/10.3402/tellusb.v64i0.15598, 2012.

Diner, D. J., Braswell, B. H., Davies, R., Gobron, N., Hu, J., Jin, Y., Kahn, R. A., Knyazikhin, Y., Loeb, N., Muller, J.-P., Nolin, A. W., Pinty, B., Schaaf, C. B., Seiz, G., and Stroeve, J.: The value of multiangle measurements for retrieving structurally and radiatively consistent properties of clouds, aerosols, and surfaces, Remote Sens. Environ., 97, 495–518, https://doi.org/10.1016/j.rse.2005.06.006, 2005.

Donovan, D. P., Klein Baltink, H., Henzing, J. S., de Roode, S. R., and Siebesma, A. P.: A depolarisation lidar-based method for the determination of liquid-cloud microphysical properties, Atmos. Meas. Tech., 8, 237–266, https://doi.org/10.5194/amt-8-237-2015, 2015.

Dowdy, A. J., Fromm, M. D., and McCarthy, N.: Pyrocumulonimbus lightning and fire ignition on Black Saturday in southeast Australia, J. Geophys. Res.-Atmos., 122, 7342–7354, https://doi.org/10.1002/2017JD026577, 2017.

Draine, B. T. and Flatau, P. J.: Discrete-Dipole Approximation For Scattering Calculations, J. Opt. Soc. Am. A, 11, 1491–1499, https://doi.org/10.1364/JOSAA.11.001491, 1994.

Drude, P., Millikan, R. A., and Mann, C. R.: The theory of optics, New York [etc.], Longmans, Green, and Co., http://file://catalog.hathitrust.org/Record/001480409 (last access: 7 October 2022), 1902.

Dubovik, O. and King, M. D.: A flexible inversion algorithm for retrieval of aerosol optical properties from Sun and sky radiance measurements, J. Geophys. Res., 105, 20673, https://doi.org/10.1029/2000JD900282, 2000.

Dubovik, O., Herman, M., Holdak, A., Lapyonok, T., Tanré, D., Deuzé, J. L., Ducos, F., Sinyuk, A., and Lopatin, A.: Statistically optimized inversion algorithm for enhanced retrieval of aerosol properties from spectral multi-angle polarimetric satellite observations, Atmos. Meas. Tech., 4, 975–1018, https://doi.org/10.5194/amt-4-975-2011, 2011.

Dubovik, O., Li, Z., Mishchenko, M. I., Tanré, D., Karol, Y., Bojkov, B., Cairns, B., Diner, D. J., Espinosa, W. R., Goloub, P., Gu, X., Hasekamp, O. P., Hong, J., Hou, W., Knobelspiesse, K. D., Landgraf, J., Li, L., Litvinov, P., Liu, Y., Lopatin, A., Marbach, T., Maring, H. B., Martins, V., Meijer, Y., Milinevsky, G., Mukai, S., Parol, F., Qiao, Y., Remer, L. A., Rietjens, J., Sano, I., Stammes, P., Stamnes, S., Sun, X., Tabary, P., Travis, L. D., Waquet, F., Xu, F., Yan, C., and Yin, D.: Polarimetric remote sensing of atmospheric aerosols: Instruments, methodologies, results, and perspectives, J. Quant. Spectrosc. Ra. Transf., 224, 474–511, https://doi.org/10.1016/j.jqsrt.2018.11.024, 2019.

Duncan, B. N., Prados, A. I., Lamsal, L. N., Liu, Y., Streets, D. G., Gupta, P., Hilsenrath, E., Kahn, R. A., Nielsen, J. E., Beyersdorf, A. J., Burton, S. P., Fiore, A. M., Fishman, J., Henze, D. K., Hostetler, C. a., Krotkov, N. A., Lee, P., Lin, M., Pawson, S., Pfister, G., Pickering, K. E., Pierce, R. B., Yoshida, Y., and Ziemba, L. D.: Satellite data of atmospheric pollution for U.S. air quality applications: Examples of applications, summary of data end-user resources, answers to FAQs, and common mistakes to avoid, Atmos. Environ., 94, 647–662, https://doi.org/10.1016/j.atmosenv.2014.05.061, 2014.

Ebben, C. J., Zorn, S. R., Lee, S.-B., Artaxo, P., Martin, S. T., and Geiger, F. M.: Stereochemical transfer to atmospheric aerosol particles accompanying the oxidation of biogenic volatile organic compounds, Geophys. Res. Lett., 38, L16807, https://doi.org/10.1029/2011GL048599, 2011.

Ebben, C. J., Shrestha, M., Martinez, I. S., Corrigan, A. L., Frossard, A. A., Song, W. W., Worton, D. R., Petäjä, T., Williams, J., Russell, L. M., Kulmala, M., Goldstein, A. H., Artaxo, P., Martin, S. T., Thomson, R. J., and Geiger, F. M.: Organic constituents on the surfaces of aerosol particles from Southern Finland, Amazonia, and California Studied by vibrational sum frequency generation, J. Phys. Chem. A, 116, 8271–8290, https://doi.org/10.1021/jp302631z, 2012.

Esposito, F., Molinaro, R., Popa, C. I., Molfese, C., Cozzolino, F., Marty, L., Taj-Eddine, K., Di Achille, G., Franzese, G., Silvestro, S., and Ori, G. G.: The role of the atmospheric electric field in the dust-lifting process, Geophys. Res. Lett., 43, 5501–5508, https://doi.org/10.1002/2016GL068463, 2016.

Evans, A. M.: Comparative Pharmacology of S(+)-Ibuprofen and (RS)-Ibuprofen, Clin. Rheumatol., 20, 9–14, https://doi.org/10.1007/BF03342662, 2001.

Facchini, M. C., Rinaldi, M., Decesari, S., Carbone, C., Finessi, E., Mircea, M., Fuzzi, S., Ceburnis, D., Flanagan, R., Nilsson, E. D., de Leeuw, G., Martino, M., Woeltjen, J., and O'Dowd, C. D.: Primary submicron marine aerosol dominated by insoluble organic colloids and aggregates, Geophys. Res. Lett., 35, https://doi.org/10.1029/2008GL034210, 2008.

Franklin, M., Kalashnikova, O. V., and Garay, M. J.: Size-resolved particulate matter concentrations derived from 4.4km-resolution size-fractionated Multi-angle Imaging SpectroRadiometer (MISR) aerosol optical depth over Southern California, Remote Sens. Environ., 196, 312–323, https://doi.org/10.1016/j.rse.2017.05.002, 2017.

Ganjitabar, H., Hadidi, R., Garcia, G. A., Nahon, L., and Powis, I.: Vibrationally-resolved photoelectron spectroscopy and photoelectron circular dichroism of bicyclic monoterpene enantiomers, J. Mol. Spectrosc., 353, 11–19, https://doi.org/10.1016/j.jms.2018.08.007, 2018.

Gao, Y. and Anderson, J. R.: Characteristics of Chinese aerosols determined by individual-particle analysis, J. Geophys. Res.-Atmos., 106, 18037–18045, https://doi.org/10.1029/2000JD900725, 2001.

Gassó, S. and Torres, O.: The role of cloud contamination, aerosol layer height and aerosol model in the assessment of the OMI near-UV retrievals over the ocean, Atmos. Meas. Tech., 9, 3031–3052, https://doi.org/10.5194/amt-9-3031-2016, 2016.

Gehrels, T., Baker, L. R., Beshore, E., Blenman, C., Burke, J. J., Castillo, N. D., Dacosta, B., Degewij, J., Doose, L. R., Fountain, J. W., Gotobed, J., Kenknight, C. E., Kingston,

R., McLaughlin, G., McMillan, R., Murphy, R., Smith, P. H., Stoll, C. P., Strickland, R. N., Tomasko, M. G., Wijesinghe, M. P., Coffeen, D. L., and Esposito, L.: Imaging Photopolarimeter on Pioneer Saturn, Science, 80, 434–439, https://doi.org/10.1126/science.207.4429.434, 1980.

Ghosh, N.: Tissue polarimetry: concepts, challenges, applications, and outlook, J. Biomed. Opt., 16, 110801, https://doi.org/10.1117/1.3652896, 2011.

Ghosh, N., Wood, M. F. G., and Vitkin, I. A.: Mueller matrix decomposition for extraction of individual polarization parameters from complex turbid media exhibiting multiple scattering, optical activity, and linear birefringence, J. Biomed. Opt., 13, 044036, https://doi.org/10.1117/1.2960934, 2008.

Gilbert, G. D. and Pernicka, J. C.: Improvement of underwater visibility by reduction of backscatter with a circular polarization technique., Appl. Opt., 6, 741–746, 1967.

Girotto, G., China, S., Bhandari, J., Gorkowski, K., Scarnato, B., Capek, T., Marinoni, A., Veghte, D., Kulkarni, G., Aiken, A., Dubey, M., and Mazzoleni, A. C.: Fractal-like Tar Ball Aggregates from Wildfire Smoke, Environ. Sci. Technol. Lett., 5, 360–365, https://doi.org/10.1021/acs.estlett.8b00229, 2018.

Glavin, D. P. and Dworkin, J. P.: Enrichment of the amino acid L-isovaline by aqueous alteration on CI and CM meteorite parent bodies, P. Natl. Acad. Sci. USA, 106, 5487–5492, https://doi.org/10.1073/pnas.0811618106, 2009.

Glavin, D. P., McLain, H. L., Dworkin, J. P., Parker, E. T., Elsila, J. E., Aponte, J. C., Simkus, D. N., Pozarycki, C. I., Graham, H. V, Nittler, L. R., and Alexander, C. M. O.: Abundant extraterrestrial amino acids in the primitive CM carbonaceous chondrite Asuka 12236, Meteorit. Planet. Sci., 55, 1979–2006, https://doi.org/10.1111/maps.13560, 2020a.

Glavin, D. P., Burton, A. S., Elsila, J. E., Aponte, J. C., and Dworkin, J. P.: The Search for Chiral Asymmetry as a Potential Biosignature in our Solar System, Chem. Rev., 120, 4660–4689, https://doi.org/10.1021/acs.chemrev.9b00474, 2020b.

Gledhill, T. M. and McCall, A.: Circular polarization by scattering from spheroidal dust grains, Mon. Not. R. Astron. Soc., 314, 123–137, https://doi.org/10.1046/j.1365-8711.2000.03323.x, 2000.

Gledhill, T. M., Sparks, W. B., Ulanowski, Z., Hough, J. H., and DasSarma, S.: ASTRO-BIOLOGICAL SIGNATURES, in: Optics of Biological Particles, edited by: Hoekstra, A., Maltsev, V., and Videen, G., 193–211 pp., Dordrecht, Springer Netherlands, https://doi.org/10.1007/978-1-4020-5502-7_6, 2007.

Goldstein, D. and Goldstein, D. H.: Polarized Light, Revised and Expanded, 2nd Edn., CRC Press, https://doi.org/10.1201/9780203911587, 2003.

González, N. J. D., Borg-Karlson, A.-K., Artaxo, P., Guenther, A., Krejci, R., Nozière, B., and Noone, K.: Primary and secondary organics in the tropical Amazonian rainforest aerosols: chiral analysis of 2-methyltetraols, Environ. Sci. Process. Impacts, 16, 1413, https://doi.org/10.1039/c4em00102h, 2014.

Gregory, R. P. and Raps, S.: The differential scattering of circularly polarized light by chloroplasts and evaluation of their true circular dichroism., Biochem. J., 142, 193–201, 1974.

Haarig, M., Walser, A., Ansmann, A., Dollner, M., Althausen, D., Sauer, D., Farrell, D., and Weinzierl, B.: Profiles of cloud condensation nuclei, dust mass concentration, and ice-nucleating-particle-relevant aerosol properties in the Saharan Air Layer over Barbados from polarization lidar and airborne in situ measurements, Atmos. Chem. Phys., 19, 13773–13788, https://doi.org/10.5194/acp-19-13773-2019, 2019.

Hansen, J. E.: Circular Polarization of Sunlight Reflected by Clouds, J. Atmos. Sci., 28, 1515–1516, https://doi.org/10.1175/1520-0469(1971)028<1515:CPOSRB>2.0.CO;2, 1971.

Hansen, J. E. and Hovenier, J. W.: Interpretation of the Polarization of Venus, J. Atmos. Sci., 31, 1137–1160, https://doi.org/10.1175/1520-0469(1974)031<1137:IOTPOV>2.0.CO;2, 1974.

Harrison, R. G., Nicoll, K. A., Ulanowski, Z., and Mather, T. A.: Self-charging of the Eyjafjallajökull volcanic ash plume, Environ. Res. Lett., 5, 24004, https://doi.org/10.1088/1748-9326/5/2/024004, 2010.

Harrison, R. G., Nicoll, K. A., Marlton, G. J., Ryder, C. L., and Bennett, A. J.: Corrigendum: Saharan dust plume charging observed over the UK 2018, Environ. Res. Lett., 13, 109502, https://doi.org/10.1088/1748-9326/aae591, 2018.

Hasekamp, O. P. and Landgraf, J.: Retrieval of aerosol properties over land surfaces: capabilities of multiple-viewing-angle intensity and polarization measurements, Appl. Opt., 46, 3332–3344, 2007.

Hasekamp, O. P., Fu, G., Rusli, S. P., Wu, L., Di Noia, A., Brugh, J. aan de, Landgraf, J., Martijn Smit, J., Rietjens, J., and van Amerongen, A.: Aerosol measurements by SPEXone on the NASA PACE mission: expected retrieval capabilities, J. Quant. Spectrosc. Ra. Transf., 227, 170–184, https://doi.org/10.1016/j.jqsrt.2019.02.006, 2019.

Herman, B. M., Caudill, T. R., Flittner, D., Thome, K. J., and Ben-David, A.: Comparison of the Gauss-Seidel spherical polarized radiative transfer code with other radiative transfer codes, Appl. Opt., 34, 4563–4572, https://doi.org/10.1364/AO.34.004563, 1995.

Herman, J. R. and Celarier, E. A.: Earth surface reflectivity climatology at 340–380 nm from TOMS data, J. Geophys. Res., 102, 28003, https://doi.org/10.1029/97JD02074, 1997.

Herman, J. R., Celarier, E., and Larko, D.: UV 380 nm reflectivity of the Earth's surface, clouds and aerosols, J. Geophys. Res., 106, 5335–5351, doi:Doi 10.1029/2000jd900584, 2001.

Herman, M., Deuzé, J.-L., Marchand, A., Roger, B., and Lallart, P.: Aerosol remote sensing from POLDER/ADEOS over the ocean: Improved retrieval using a nonspherical particle model, J. Geophys. Res.-Atmos., 110, D10S02, https://doi.org/10.1029/2004JD004798, 2005.

Hodzic, A., Kasibhatla, P. S., Jo, D. S., Cappa, C. D., Jimenez, J. L., Madronich, S., and Park, R. J.: Rethinking the global secondary organic aerosol (SOA) budget: stronger production, faster removal, shorter lifetime, Atmos. Chem. Phys., 16, 7917–7941, https://doi.org/10.5194/acp-16-7917-2016, 2016.

Holloway, T., Miller, D., Anenberg, S., Diao, M., Duncan, B., Fiore, A. M., Henze, D. K., Hess, J., Kinney, P. L., Liu, Y., Neu, J. L., O'Neill, S. M., Odman, M. T., Pierce, R. B., Russell, A. G., Tong, D., West, J. J., and Zondlo, M. A.: Satellite Monitoring for Air Quality and Health, Annu. Rev. Biomed. Data Sci., 4, 417–447, https://doi.org/10.1146/annurev-biodatasci-110920-093120, 2021.

Hough, J. H.: High sensitivity polarimetry: techniques and applications BT – Polarimetric Detection, Characterization and Remote

Sensing, edited by: Mishchenko, M. I., Yatskiv, Y. S., Rosenbush, V. K., and Videen, G., 177–204, Springer Netherlands, Dordrecht, https://doi.org/10.1007/978-94-007-1636-0, 2011.

Hough, J. H., Lucas Patty, C. H., Bailey, J. A., Tamura, M., Hirst, E., Harrison, D., and Bartholomew-Biggs, M.: PlanetPol: A Very High Sensitivity Polarimeter, Publ. Astron. Soc. Pacific, 118, 1302–1318, https://doi.org/10.1086/507955, 2006.

Hsu, N. C., Jeong, M.-J., Bettenhausen, C., Sayer, A. M., Hansell, R., Seftor, C. J., Huang, J., and Tsay, S.-C.: Enhanced Deep Blue aerosol retrieval algorithm: The second generation, J. Geophys. Res.-Atmos., 118, 9296–9315, https://doi.org/10.1002/jgrd.50712, 2013.

Hu, Y., Yang, P., Lin, B., Gibson, G., and Hostetler, C.: Discriminating between spherical and non-spherical scatterers with lidar using circular polarization: a theoretical study, J. Quant. Spectrosc. Ra. Transf., 79–80, 757–764, https://doi.org/10.1016/S0022-4073(02)00320-5, 2003.

Inness, A., Ades, M., Agustí-Panareda, A., Barré, J., Benedictow, A., Blechschmidt, A.-M., Dominguez, J. J., Engelen, R., Eskes, H., Flemming, J., Huijnen, V., Jones, L., Kipling, Z., Massart, S., Parrington, M., Peuch, V.-H., Razinger, M., Remy, S., Schulz, M., and Suttie, M.: The CAMS reanalysis of atmospheric composition, Atmos. Chem. Phys., 19, 3515–3556, https://doi.org/10.5194/acp-19-3515-2019, 2019.

Ippolitov, I. I., Kabanova, M. V., Nagorskii, P. M., Pkhalagov, Y. A., and Smirnov, S. V.: Diurnal variations in the electrical field intensity under smoke from forest fires, Dokl. Earth Sci., 453, 1137–1140, https://doi.org/10.1134/S1028334X1311010X, 2013.

Jethva, H. and Torres, O.: A comparative evaluation of Aura-OMI and SKYNET near-UV single-scattering albedo products, Atmos. Meas. Tech., 12, 6489–6503, https://doi.org/10.5194/amt-12-6489-2019, 2019.

Jethva, H., Torres, O., and Ahn, C.: Global assessment of OMI aerosol single-scattering albedo using ground-based AERONET inversion, J. Geophys. Res.-Atmos., 119, 9020–9040, https://doi.org/10.1002/2014JD021672, 2014.

Kahn, R. A. and Gaitley, B. J.: An analysis of global aerosol type as retrieved by MISR, J. Geophys. Res.-Atmos., (February), 120, 4248–4281, https://doi.org/10.1002/2015JD023322, 2015.

Kamra, A. K.: Measurements of the electrical properties of dust storms, J. Geophys. Res., 77, 5856–5869, https://doi.org/10.1029/JC077i030p05856, 1972.

Kawabata, K., Coffeen, D. L., Hansen, J. E., Lane, W. A., Sato, M., and Travis, L. D.: Cloud and haze properties from Pioneer Venus polarimetry, J. Geophys. Res., 85, 8129, https://doi.org/10.1029/JA085iA13p08129, 1980.

Kawata, Y.: Circular polarization of sunlight reflected by planetary atmospheres, Icarus, 33, 217–232, https://doi.org/10.1016/0019-1035(78)90035-0, 1978.

Keller, D., Bustamante, C., Maestre, M. F., and Tinoco, I.: Imaging of optically active biological structures by use of circularly polarized light, P. Natl. Acad. Sci. USA, 82, 401–405, https://doi.org/10.1073/pnas.82.2.401, 1985.

Kellogg, C. A. and Griffin, D. W.: Aerobiology and the global transport of desert dust, Trends Ecol. Evol., 21, 638–644, https://doi.org/10.1016/j.tree.2006.07.004, 2006.

Kemp, J., Henson, G., Steiner, C., and Powell, E.: The optical polarization of the Sun measured at a sensitivity of parts in ten million, Nature, 326, 270–273, https://doi.org/10.1038/326270a0, 1987.

Kemp, J. C., Wolstencroft, R. D., and SWEDLUND, J. B.: Circular Polarization: Jupiter and Other Planets, Nature, 232, 165–168, https://doi.org/10.1038/232165a0, 1971.

Kemppinen, O., Nousiainen, T., and Jeong, G. Y.: Effects of dust particle internal structure on light scattering, Atmos. Chem. Phys., 15, 12011–12027, https://doi.org/10.5194/acp-15-12011-2015, 2015.

Kim, J. H. and Scialli, A. R.: Thalidomide: The Tragedy of Birth Defects and the Effective Treatment of Disease, Toxicol. Sci., 122, 1–6, https://doi.org/10.1093/toxsci/kfr088, 2011.

Knobelspiesse, K., Cairns, B., Mishchenko, M., Chowdhary, J., Tsigaridis, K., van Diedenhoven, B., Martin, W., Ottaviani, M., and Alexandrov, M.: Analysis of fine-mode aerosol retrieval capabilities by different passive remote sensing instrument designs, Opt. Express, 20, 21457, https://doi.org/10.1364/OE.20.021457, 2012.

Knobelspiesse, K., Ibrahim, A., Franz, B., Bailey, S., Levy, R., Ahmad, Z., Gales, J., Gao, M., Garay, M., Anderson, S., and Kalashnikova, O.: Analysis of simultaneous aerosol and ocean glint retrieval using multi-angle observations, Atmos. Meas. Tech., 14, 3233–3252, https://doi.org/10.5194/amt-14-3233-2021, 2021.

Kok, J. F. and Renno, N. O.: Electrostatics in Wind-Blown Sand, Phys. Rev. Lett., 100, 014501, https://doi.org/10.1103/PhysRevLett.100.014501, 2008.

Kokhanovsky, A. A.: Radiative transfer in chiral random media, Phys. Rev. E, 60, 4899–4907, https://doi.org/10.1103/PhysRevE.60.4899, 1999.

Kokhanovsky, A. A.: Theoretical modelling of CD and ORD spectra of suspensions with large nonspherical particles, J. Opt. A Pure Appl. Opt., 4, 288–292, https://doi.org/10.1088/1464-4258/4/3/312, 2002.

Kolokolova, L. and Nagdimunov, L.: Comparative analysis of polarimetric signatures of aligned and optically active ("homochiral") dust particles, Planet. Space Sci., 100, 57–63, https://doi.org/10.1016/j.pss.2014.01.002, 2014.

Kolokolova, L., Petrova, E., and Kimura, H.: Effects of Interaction of Electromagnetic Waves in Complex Particles, edited by: Zhurbenko, V., InTech., 2011.

Kunnen, B., Macdonald, C., Doronin, A., Jacques, S., Eccles, M., and Meglinski, I.: Application of circularly polarized light for non-invasive diagnosis of cancerous tissues and turbid tissue-like scattering media, J. Biophotonics, 8, 317–323, https://doi.org/10.1002/jbio.201400104, 2015.

Kuznetsova, M., Lee, C., and Aller, J.: Characterization of the proteinaceous matter in marine aerosols, Mar. Chem., 96, 359–377, https://doi.org/10.1016/j.marchem.2005.03.007, 2005.

Lakhtakia, A.: Selected Papers on Natural Optical Activity, edited by: Lakhtakia, A., (Milestone), Bellingham, WA, PIE Optical Engineering Press, https://spie.org/Publications/Book/2315 (last access: 4 October 2022), 1990.

Lane, S. J., James, M. R., and Gilbert, J. S.: Electrostatic phenomena in volcanic eruptions, J. Phys. Conf. Ser., 301, 12004, https://doi.org/10.1088/1742-6596/301/1/012004, 2011.

LaRoche, K. T. and Lang, T. J.: Observations of Ash, Ice, and Lightning within Pyrocumulus Clouds Using Polarimetric NEXRAD Radars and the National Lightning Detection Network, Mon. Weather Rev., 145, 4899–4910, https://doi.org/10.1175/MWR-D-17-0253.1, 2017.

Leck, C. and Bigg, E. K.: Biogenic particles in the surface microlayer and overlaying atmosphere in the central Arctic Ocean during summer, Tellus B Chem. Phys. Meteorol., 57, 305–316, https://doi.org/10.3402/tellusb.v57i4.16546, 2005.

Lee, B. H., Lopez-Hilfiker, F. D., D'Ambro, E. L., Zhou, P., Boy, M., Petäjä, T., Hao, L., Virtanen, A., and Thornton, J. A.: Semi-volatile and highly oxygenated gaseous and particulate organic compounds observed above a boreal forest canopy, Atmos. Chem. Phys., 18, 11547–11562, https://doi.org/10.5194/acp-18-11547-2018, 2018.

Levy, R. C., Mattoo, S., Munchak, L. A., Remer, L. A., Sayer, A. M., Patadia, F., and Hsu, N. C.: The Collection 6 MODIS aerosol products over land and ocean, Atmos. Meas. Tech., 6, 2989–3034, https://doi.org/10.5194/amt-6-2989-2013, 2013.

Levy, R. C., Munchak, L. A., Mattoo, S., Patadia, F., Remer, L. A., and Holz, R. E.: Towards a long-term global aerosol optical depth record: applying a consistent aerosol retrieval algorithm to MODIS and VIIRS-observed reflectance, Atmos. Meas. Tech., 8, 4083–4110, https://doi.org/10.5194/amt-8-4083-2015, 2015.

Lewis, G. D., Jordan, D. L., and Roberts, P. J.: Backscattering target detection in a turbid medium by polarization discrimination, Appl. Opt., 38, 3937, https://doi.org/10.1364/AO.38.003937, 1999.

Li, L., Dubovik, O., Derimian, Y., Schuster, G. L., Lapyonok, T., Litvinov, P., Ducos, F., Fuertes, D., Chen, C., Li, Z., Lopatin, A., Torres, B., and Che, H.: Retrieval of aerosol components directly from satellite and ground-based measurements, Atmos. Chem. Phys., 19, 13409–13443, https://doi.org/10.5194/acp-19-13409-2019, 2019.

Li, P., Lv, D., He, H., and Ma, H.: Separating azimuthal orientation dependence in polarization measurements of anisotropic media, Opt. Express, 26, 3791, https://doi.org/10.1364/OE.26.003791, 2018.

Li, Z., Xie, Y., Li, L., and Zhang, Y.: Remote Sensing of Atmospheric Aerosol Composition and Species, in: Remote Sensing of Atmospheric Aerosol Composition and Species, SPIE, https://doi.org/10.1117/3.2537401.ch1, 2019.

Liu, J. and Kattawar, G. W.: Detection of dinoflagellates by the light scattering properties of the chiral structure of their chromosomes, J. Quant. Spectrosc. Ra. Transf., 131, 24–33, https://doi.org/10.1016/j.jqsrt.2013.02.012, 2013.

Liu, Y. and Diner, D. J.: Multi-Angle Imager for Aerosols: A Satellite Investigation to Benefit Public Health, Public Health Rep., 132, 14–17, https://doi.org/10.1177/0033354916679983, 2016.

Lofftus, K., Hunt, A. J., Quinby-Hunt, M. S., Livolant, F., and Maestre, M. F.: Immobilization Of Unicellular Marine Organisms For Optical Characterization: A New Method, in: Proc. SPIE 0925, Ocean Optics IX, edited by: Blizard, M. A., 334–343, 1988.

Lucas Patty, C. H., Snik, F., and Visser, L.: A high-sensitivity circular spectropolarimeter for remote sensing of homochirality in photosynthetic organisms (Conference Presentation), in: Polarization Science and Remote Sensing VIII, edited by: Snik, F. and Shaw, J. A., p. 35, SPIE, 2017.

Lucas Patty, C. H., Luo, D. A., Snik, F., Ariese, F., Buma, W. J., ten Kate, I. L., van Spanning, R. J. M., Sparks, W. B., Germer, T. A., Garab, G., and Kudenov, M. W.: Imaging linear and circular polarization features in leaves with complete Mueller matrix polarimetry, Biochim. Biophys. Acta – Gen. Subj., 1862, 1350–1363, https://doi.org/10.1016/j.bbagen.2018.03.005, 2018a.

Lucas Patty, C. H., ten Kate, I. L., Sparks, W. B., and Snik, F.: Remote Sensing of Homochirality: A Proxy for the Detection of Extraterrestrial Life, in: Chiral Analysis, pp. 29–69, Elsevier, 2018b.

Lucas Patty, C. H., Ariese, F., Buma, W. J., ten Kate, I. L., van Spanning, R. J. M., and Snik, F.: Circular spectropolarimetric sensing of higher plant and algal chloroplast structural variations, Photosynth. Res., 140, 129–139, https://doi.org/10.1007/s11120-018-0572-2, 2019a.

Lucas Patty, C. H., ten Kate, I. L., Buma, W. J., van Spanning, R. J. M., Steinbach, G., Ariese, F., and Snik, F.: Circular Spectropolarimetric Sensing of Vegetation in the Field: Possibilities for the Remote Detection of Extraterrestrial Life, Astrobiology, ast.2019.2050, https://doi.org/10.1089/ast.2019.2050, 2019b.

Lucas Patty, C. H., Kühn, J. G., Lambrev, P. H., Spadaccia, S., Hoeijmakers, H. J., Keller, C., Mulder, W., Pallichadath, V., Frans, O., Snik, F., Stam, D. M., Pommerol, A., and Demory, B: Biosignatures of the Earth, A&A, 651, https://doi.org/10.1051/0004-6361/202140845, 2021.

MacDermott, A. J.: Distinguishing the chiral signature of life in the solar system and beyond, in: Instruments, Methods, and Missions for the Investigation of Extraterrestrial Microorganisms Richard B. Hoover, vol. 3111, edited by: Hoover, R. B., 272–279, 1997.

MacKenzie, S. M., Neveu, M., Davila, A. F., Lunine, J. I., Craft, K. L., Cable, M. L., Phillips-Lander, C. M., Hofgartner, J. D., Eigenbrode, J. L., Waite, J. H., Glein, C. R., Gold, R., Greenauer, P. J., Kirby, K., Bradburne, C., Kounaves, S. P., Malaska, M. J., Postberg, F., Patterson, G. W., Porco, C., Núñez, J. I., German, C., Huber, J. A., McKay, C. P., de Vera, J.-P., Brucato, J. R., and Spilker, L. J.: The Enceladus Orbilander Mission Concept: Balancing Return and Resources in the Search for Life, Planet. Sci. J., 2, 77, https://doi.org/10.3847/psj/abe4da, 2021.

Magzamen, S., Gan, R. W., Liu, J., O'Dell, K., Ford, B., Berg, K., Bol, K., Wilson, A., Fischer, E. V., and Pierce, J. R.: Differential Cardiopulmonary Health Impacts of Local and Long-Range Transport of Wildfire Smoke, GeoHealth, 5, e2020GH000330, https://doi.org/10.1029/2020GH000330, 2021.

Mallios, S. A., Daskalopoulou, V., and Amiridis, V.: Orientation of non spherical prolate dust particles moving vertically in the Earth's atmosphere, J. Aerosol Sci., 151, 105657, https://doi.org/10.1016/j.jaerosci.2020.105657, 2021.

Manisalidis, I., Stavropoulou, E., Stavropoulos, A., and Bezirtzoglou, E.: Environmental and Health Impacts of Air Pollution: A Review, Front. Public Heal., 8, 14, https://doi.org/10.3389/fpubh.2020.00014, 2020.

Maring, H. B.: Vertical distributions of dust and sea-salt aerosols over Puerto Rico during PRIDE measured from a light aircraft, J. Geophys. Res., 108, 8587, https://doi.org/10.1029/2002JD002544, 2003.

Martin, W. E., Hesse, E., Hough, J. H., Sparks, W. B., Cockell, C. S., Ulanowski, Z., Germer, T. A., and Kaye, P. H.: Polarized optical scattering signatures from biological materials, J. Quant. Spectrosc. Radiat. Transf., 111, 2444–2459, https://doi.org/10.1016/j.jqsrt.2010.07.001, 2010.

Martin, W. E., Hesse, E., Hough, J. H., and Gledhill, T. M.: High-sensitivity Stokes spectropolarime-

try on cyanobacteria, J. Quant. Spectrosc. Ra. Transf., https://doi.org/10.1016/j.jqsrt.2015.10.014, 2016.

Martinez, I. S., Peterson, M. D., Ebben, C. J., Hayes, P. L., Artaxo, P., Martin, S. T., and Geiger, F. M.: On molecular chirality within naturally occurring secondary organic aerosol particles from the central Amazon Basin, Phys. Chem. Chem. Phys., 13, 12114, https://doi.org/10.1039/c1cp20428a, 2011.

McCoy, D. T., Burrows, S. M., Wood, R., Grosvenor, D. P., Elliott, S. M., Ma, P.-L., Rasch, P. J., and Hartmann, D. L.: Natural aerosols explain seasonal and spatial patterns of Southern Ocean cloud albedo, Sci. Adv., 1, e1500157, https://doi.org/10.1126/sciadv.1500157, 2015.

Meierhenrich, U. J., Thiemann, W. H.-P., Barbier, B., Brack, A., Alcaraz, C., Nahon, L., and Wolstencroft, R.: Circular Polarization of Light by Planet Mercury and Enantiomorphism of its Surface Minerals, Orig. life Evol. Biosph., 32, 181–190, https://doi.org/10.1023/A:1016028930938, 2002.

Mhawish, A., Kumar, M., Mishra, A. K., Srivastava, P. K., and Banerjee, T.: Remote Sensing of Aerosols From Space: Retrieval of Properties and Applications, in: Remote Sensing of Aerosols, Clouds, and Precipitation, edited by: Islam, T., Hu, Y., Kokhanovsky, A., and Wang, J., pp. 45–83, Elsevier, 2018.

Mishchenko, M. I.: Electromagnetic Scattering by Particles and Particle Groups: An Introduction, Cambridge University Press, Cambridge, https://doi.org/10.1017/CBO9781139019064, 2014.

Mishchenko, M. I. and Hovenier, J. W.: Depolarization of light backscattered by randomly oriented nonspherical particles, Opt. Lett., 20, 1356, https://doi.org/10.1364/OL.20.001356, 1995.

Mishchenko, M. I. and Yurkin, M. A.: On the concept of random orientation in far-field electromagnetic scattering by nonspherical particles, Opt. Lett., 42, 494, https://doi.org/10.1364/OL.42.000494, 2017.

Mishchenko, M. I., Hovenier, J. W., and Travis, L. D. (Eds.): Light Scattering by Nonspherical Particles: Theory, Measurements, and Applications, Measurement Sci. Technol., 11, 1827–1827, https://doi.org/10.1088/0957-0233/11/12/705, 2000.

Moore, R. H., Karydis, V. A., Capps, S. L., Lathem, T. L., and Nenes, A.: Droplet number uncertainties associated with CCN: an assessment using observations and a global model adjoint, Atmos. Chem. Phys., 13, 4235–4251, https://doi.org/10.5194/acp-13-4235-2013, 2013.

Muñoz, O., Volten, H., de Haan, J. F., Vassen, W., and Hovenier, J. W.: Experimental determination of scattering matrices of randomly oriented fly ash and clay particles at 442 and 633 nm, J. Geophys. Res.-Atmos., 106, 22833–22844, https://doi.org/10.1029/2000JD000164, 2001.

Murdin, P.: Encyclopedia of Astronomy & Astrophysics, 1st Edn., Boca Raton, CRC Press, https://www.taylorfrancis.com/books/edit/10.1201/9781003220435/encyclopedia-astronomy-astrophysics-paul-murdin (last access: 4 October 2022), 2001.

Myriokefalitakis, S., Fanourgakis, G., and Kanakidou, M.: The Contribution of Bioaerosols to the Organic Carbon Budget of the Atmosphere BT – Perspectives on Atmospheric Sciences, edited by: Karacostas, T., Bais, A., and Nastos, P. T., 845–851, Springer International Publishing, Cham, 2017.

Nafie, L. A.: Circular polarization spectroscopy of chiral molecules, J. Mol. Struct., 347, 83–100, https://doi.org/10.1016/0022-2860(95)08538-7, 1995.

Nagorskiy, P. M., Pustovalov, K. N., and Smirnov, S. V.: Smoke Plumes from Wildfires and the Electrical State of the Surface Air Layer, Atmos. Ocean. Opt., 35, 387–393, https://doi.org/10.1134/S1024856022040133, 2022.

NASA: The Pioneer Missions, https://www.nasa.gov/centers/ames/missions/archive/pioneer.html, last access: 24 August 2021.

Neupert, W., Brugger, R., Euchenhofer, C., Brune, K., and Geisslinger, G.: Effects of ibuprofen enantiomers and its coenzyme A thioesters on human prostaglandin endoperoxide synthases, Br. J. Pharmacol., 122, 487–492, https://doi.org/10.1038/sj.bjp.0701415, 1997.

Neveu, M., Anbar, A. D., Davila, A. F., Glavin, D. P., MacKenzie, S. M., Phillips-Lander, C. M., Sherwood, B., Takano, Y., Williams, P., and Yano, H.: Returning Samples From Enceladus for Life Detection , Front. Astron. Sp. Sci., 7, 26, https://doi.org/10.3389/fspas.2020.00026, 2020.

Nicolet, M., Schnaiter, M., and Stetzer, O.: Circular depolarization ratios of single water droplets and finite ice circular cylinders: a modeling study, Atmos. Chem. Phys., 12, 4207–4214, https://doi.org/10.5194/acp-12-4207-2012, 2012.

Nicoll, K. A., Harrison, R. G., and Ulanowski, Z.: Observations of Saharan dust layer electrification, Environ. Res. Lett., 6, 14001, https://doi.org/10.1088/1748-9326/6/1/014001, 2010.

Nouri, S. A., Gregory, D. A., and Fuller, K.: Development of an angle-scanning spectropolarimeter: Preliminary results, J. Quant. Spectrosc. Ra. Transf., 206, 342–354, https://doi.org/10.1016/j.jqsrt.2017.11.024, 2018.

Noziere, B., González, N. J. D., Borg-Karlson, A. K., Pei, Y., Redeby, J. P., Krejci, R., Dommen, J., Prevot, A. S. H., and Anthonsen, T.: Atmospheric chemistry in stereo: A new look at secondary organic aerosols from isoprene, Geophys. Res. Lett., 38, 138, https://doi.org/10.1029/2011GL047323, 2011.

O'Dowd, C. D., Facchini, M. C., Cavalli, F., Ceburnis, D., Mircea, M., Decesari, S., Fuzzi, S., Yoon, Y. J., Putaud, J., Dowd, C. D. O., Facchini, M. C., Cavalli, F., Ceburnis, D., Mircea, M., Decesari, S., Fuzzi, S., Yoon, Y. J., and Putaud, J.: Biogenically driven organic contribution to marine aerosol, Nature, 431, 676, https://doi.org/10.1038/nature02959, 2004.

Okada, K., Heintzenberg, J., Kai, K., and Qin, Y.: Shape of atmospheric mineral particles collected in three Chinese arid-regions, Geophys. Res. Lett., 28, 3123–3126, https://doi.org/10.1029/2000GL012798, 2001.

Omar, A. H., Winker, D. M., Vaughan, M. A., Hu, Y., Trepte, C. R., Ferrare, R. A., Lee, K.-P., Hostetler, C. A., Kittaka, C., Rogers, R. R., Kuehn, R. E., and Liu, Z.: The CALIPSO Automated Aerosol Classification and Lidar Ratio Selection Algorithm, J. Atmos. Ocean. Technol., 26, 1994–2014, https://doi.org/10.1175/2009JTECHA1231.1, 2009.

Pan, Y.-L., Kalume, A., Arnold, J., Beresnev, L., Wang, C., Rivera, D. N., Crown, K. K., and Santarpia, J.: Measurement of circular intensity differential scattering (CIDS) from single airborne aerosol particles for bioaerosol detection and identification, Opt. Express, 30, 1442–1451, https://doi.org/10.1364/OE.448288, 2022.

Paschou, P., Siomos, N., Tsekeri, A., Louridas, A., Georgoussis, G., Freudenthaler, V., Binietoglou, I., Tsaknakis, G., Tavernarakis, A., Evangelatos, C., von Bismarck, J., Kanitz, T., Meleti, C., Marinou, E., and Amiridis, V.: The eVe reference polarisation lidar system for the calibration and validation of

the Aeolus L2A product, Atmos. Meas. Tech., 15, 2299–2323, https://doi.org/10.5194/amt-15-2299-2022, 2022.

Pendleton, J. D. and Rosen, D. L.: Light Scattering from an Optically Active Sphere into a Circular Aperture, Appl. Opt., 37, 7897, https://doi.org/10.1364/AO.37.007897, 1998.

Perrin, F.: Polarization of Light Scattered by Isotropic Opalescent Media, J. Chem. Phys., 10, 415, https://doi.org/10.1063/1.1723743, 1942.

Perring, A. E., Schwarz, J. P., Baumgardner, D., Hernandez, M. T., Spracklen, D. V, Heald, C. L., Gao, R. S., Kok, G., McMeeking, G. R., McQuaid, J. B., and Fahey, D. W.: Airborne observations of regional variation in fluorescent aerosol across the United States, J. Geophys. Res.-Atmos., 2014, JD022495, https://doi.org/10.1002/2014JD022495, 2014.

Petäjä, T., O'Connor, E. J., Moisseev, D., Sinclair, V. A., Manninen, A. J., Väänänen, R., von Lerber, A., Thornton, J. A., Nicoll, K., Petersen, W., Chandrasekar, V., Smith, J. N., Winkler, P. M., Krüger, O., Hakola, H., Timonen, H., Brus, D., Laurila, T., Asmi, E., Riekkola, M.-L., Mona, L., Massoli, P., Engelmann, R., Komppula, M., Wang, J., Kuang, C., Bäck, J., Virtanen, A., Levula, J., Ritsche, M., and Hickmon, N.: BAECC: A Field Campaign to Elucidate the Impact of Biogenic Aerosols on Clouds and Climate, B. Am. Meteorol. Soc., 97, 1909–1928, https://doi.org/10.1175/BAMS-D-14-00199.1, 2016.

Phalagov, Y. A., Ippolitov, I. I., Nagorskii, P. M., Odintsov, S. L., Panchenko, M. V., Smirnov, S. V., and Uzhegov, V. N.: Relation of anomalous atmospheric conditions to electric field variation, Atmos. Ocean. Opt., 22, 113–117, https://doi.org/10.1134/S1024856009010163, 2009.

Pospergelis, M. M.: Spectroscopic Measurements of the Four Stokes Parameters for Light Scattered by Natural Objects, Sov. Physics-Astronomy, 12, 973, 1969.

Purvinis, G., Cameron, B. D., and Altrogge, D. M.: Noninvasive Polarimetric-Based Glucose Monitoring: An in Vivo Study, J. Diabetes Sci. Technol., 5, 380–387, https://doi.org/10.1177/193229681100500227, 2011.

Qi, J. and Elson, D. S.: Mueller polarimetric imaging for surgical and diagnostic applications: a review, J. Biophotonics, 10, 950–982, https://doi.org/10.1002/jbio.201600152, 2017.

Quinby-Hunt, M. S., Erskine, L. L., and Hunt, A. J.: Polarized light scattering by aerosols in the marine atmospheric boundarylayer, Appl. Opt., 36, 5168–5184, https://doi.org/10.1364/AO.36.005168, 1997.

Remer, L. A., Kleidman, R. G., Levy, R. C., Kaufman, Y. J., Tanré, D., Mattoo, S., Martins, J. V., Ichoku, C., Koren, I., Yu, H., and Holben, B. N.: Global aerosol climatology from the MODIS satellite sensors, J. Geophys. Res., 113, D14S07, https://doi.org/10.1029/2007JD009661, 2008.

Remer, L. A., Knobelspiesse, K., Zhai, P.-W., Xu, F., Kalashnikova, O. V, Chowdhary, J., Hasekamp, O. P., Dubovik, O., Wu, L., Ahmad, Z., Boss, E., Cairns, B., Coddington, O., Davis, A. B., Dierssen, H. M., Diner, D. J., Franz, B., Frouin, R., Gao, B.-C., Ibrahim, A., Levy, R. C., Martins, J. V., Omar, A. H., and Torres, O.: Retrieving Aerosol Characteristics From the PACE Mission, Part 2: Multi-Angle and Polarimetry , Front. Environ. Sci. , 7, 94 https://doi.org/10.3389/fenvs.2019.00094, 2019.

Rogers, C. and Martin, P. G.: On the shape of interstellar grains, Astrophys. J., 228, 450–464, https://doi.org/10.1086/156866, 1979.

Rosen, D. L.: Remote Biodetection Method Using Circular Dichroism, Appl. Spectrosc., 47, 1887–1891, https://doi.org/10.1366/0003702934066073, 1993.

Rosenbush, V., Kiselev, N., Shakhovskoy, N., Kolesnikov, S., and Breus, V.: Circular and linear polarization of comet C/2001 Q4 (NEAT), Why circular polarization in comets is predominantly left-handed?, Conf. Electromagn. Light Scatt., 4, 181–184, https://doi.org/10.1615/ICHMT.2007.ConfElectromagLigScat.480, 2007.

Rubin, N. A., D'Aversa, G., Chevalier, P., Shi, Z., Chen, W. T., and Capasso, F.: Matrix Fourier optics enables a compact full-Stokes polarization camera, Science, 80, 365, https://doi.org/10.1126/science.aax1839, 2019.

Russell, P. B., Kacenelenbogen, M., Livingston, J. M., Hasekamp, O. P., Burton, S. P., Schuster, G. L., Johnson, M. S., Knobelspiesse, K. D., Redemann, J., Ramachandran, S., and Holben, B. N.: A multiparameter aerosol classification method and its application to retrievals from spaceborne polarimetry, J. Geophys. Res.-Atmos., 119, 9838–9863, https://doi.org/10.1002/2013JD021411, 2014.

Ryder, C. L., Highwood, E. J., Rosenberg, P. D., Trembath, J., Brooke, J. K., Bart, M., Dean, A., Crosier, J., Dorsey, J., Brindley, H., Banks, J., Marsham, J. H., McQuaid, J. B., Sodemann, H., and Washington, R.: Optical properties of Saharan dust aerosol and contribution from the coarse mode as measured during the Fennec 2011 aircraft campaign, Atmos. Chem. Phys., 13, 303–325, https://doi.org/10.5194/acp-13-303-2013, 2013.

Salma, I., Mészáros, T., Maenhaut, W., Vass, E., and Majer, Z.: Chirality and the origin of atmospheric humic-like substances, Atmos. Chem. Phys., 10, 1315–1327, https://doi.org/10.5194/acp-10-1315-2010, 2010.

Samaké, A., Jaffrezo, J.-L., Favez, O., Weber, S., Jacob, V., Albinet, A., Riffault, V., Perdrix, E., Waked, A., Golly, B., Salameh, D., Chevrier, F., Oliveira, D. M., Bonnaire, N., Besombes, J.-L., Martins, J. M. F., Conil, S., Guillaud, G., Mesbah, B., Rocq, B., Robic, P.-Y., Hulin, A., Le Meur, S., Descheemaecker, M., Chretien, E., Marchand, N., and Uzu, G.: Polyols and glucose particulate species as tracers of primary biogenic organic aerosols at 28 French sites, Atmos. Chem. Phys., 19, 3357–3374, https://doi.org/10.5194/acp-19-3357-2019, 2019.

Sanchez, K. J., Chen, C.-L., Russell, L. M., Betha, R., Liu, J., Price, D. J., Massoli, P., Ziemba, L. D., Crosbie, E. C., Moore, R. H., Müller, M., Schiller, S. A., Wisthaler, A., Lee, A. K. Y., Quinn, P. K., Bates, T. S., Porter, J., Bell, T. G., Saltzman, E. S., Vaillancourt, R. D., and Behrenfeld, M. J.: Substantial Seasonal Contribution of Observed Biogenic Sulfate Particles to Cloud Condensation Nuclei, Sci. Rep., 8, 3235, https://doi.org/10.1038/s41598-018-21590-9, 2018.

Sassen, K.: Boreal tree pollen sensed by polarization lidar: Depolarizing biogenic chaff, Geophys. Res. Lett., 35, https://doi.org/10.1029/2008GL035085, 2008.

Savenkov, S. N.: Mueller-matrix characterization of biological tissues BT – Polarimetric Detection, in: Characterization and Remote Sensing, edited by: Mishchenko, M. I., Yatskiv, Y. S., Rosenbush, V. K., and Videen, G., 437–472 pp., Dordrecht, Springer Netherlands, https://doi.org/10.1007/978-94-007-1636-0_17, 2011.

Sayer, A. M., Smirnov, A., Hsu, N. C., and Holben, B. N.: A pure marine aerosol model, for use in remote

sensing applications, J. Geophys. Res.-Atmos., 117, D5, https://doi.org/10.1029/2011JD016689, 2012.

Sayer, A. M., Hsu, N. C., Bettenhausen, C., and Jeong, M.-J.: Validation and uncertainty estimates for MODIS Collection 6 "Deep Blue" aerosol data, J. Geophys. Res.-Atmos., 118, 7864–7872, https://doi.org/10.1002/jgrd.50600, 2013.

Sayer, A. M., Hsu, N. C., Lee, J., Kim, W. V, Dubovik, O., Dutcher, S. T., Huang, D., Litvinov, P., Lyapustin, A., Tackett, J. L., and Winker, D. M.: Validation of SOAR VIIRS Over-Water Aerosol Retrievals and Context Within the Global Satellite Aerosol Data Record, J. Geophys. Res.-Atmos., 123, 13413–496526, https://doi.org/10.1029/2018JD029465, 2018.

Schmidt, T. H.: Elliptical Polarization by Light Scattering by Submicron Spheroids, in: Interstellar Dust and Related Topics, edited by: Greenberg, J. M. and Van De Hulst, H. C., 131–137, Springer Netherlands, Dordrecht, 1973.

Schutgens, N., Dubovik, O., Hasekamp, O., Torres, O., Jethva, H., Leonard, P. J. T., Litvinov, P., Redemann, J., Shinozuka, Y., de Leeuw, G., Kinne, S., Popp, T., Schulz, M., and Stier, P.: AEROCOM and AEROSAT AAOD and SSA study – Part 1: Evaluation and intercomparison of satellite measurements, Atmos. Chem. Phys., 21, 6895–6917, https://doi.org/10.5194/acp-21-6895-2021, 2021.

Shang, X., Baars, H., Stachlewska, I. S., Mattis, I., and Komppula, M.: Pollen observations at four EARLINET stations during the ACTRIS-COVID-19 campaign, Atmos. Chem. Phys., 22, 3931–3944, https://doi.org/10.5194/acp-22-3931-2022, 2022.

Shapiro, D. B., Quinby-Hunt, M. S. and Hunt, A. J.: Origin of the induced circular polarization in the light scattering from a dinoflagellate, in: Proc. SPIE 1302, Ocean Optics X, vol. 1302, edited by: Spinrad, R. W., 281–289, 1990.

Shapiro, D. B., Hunt, A. J., Quinby-Hunt, M. S., and Hull, P. G.: Circular polarization effects in the light scattering from single and suspensions of dinoflagellates, in: SPIEVol. 1537 Underwater Imaging, Photography, and Visibility, vol. 1537, edited by: Spinrad, R. W., 30–41, 1991.

Shi, W., Fan, F., Zhang, Z., Zhang, T., Li, S., Wang, X., and Chang, S.: Terahertz Sensing for R/S Chiral Ibuprofen via All-Dielectric Metasurface with Higher-Order Resonance, Appl. Sci. , 11, 8892, https://doi.org/10.3390/app11198892, 2021.

Slonaker, R. L., Takano, Y., Liou, K.-N., and Ou, S.-C.: Circular polarization signal for aerosols and clouds, in: Proc. SPIE, vol. 5890, edited by: Huang, H.-L. A., Bloom, H. J., Xu, X., and Dittberner, G. J., 58900B–58900B–8, 2005.

Sloot, P. M. A., Hoekstra, A. G., van der Liet, H., and Figdor, C. G.: Scattering matrix elements of biological particles measured in a flow through system: theory and practice, Appl. Opt., 28, 1752, https://doi.org/10.1364/AO.28.001752, 1989.

Smith, S. W.: Chiral Toxicology: It's the Same Thing... Only Different, Toxicol. Sci., 110, 4–30, https://doi.org/10.1093/toxsci/kfp097, 2009.

Song, W., Staudt, M., Bourgeois, I., and Williams, J.: Laboratory and field measurements of enantiomeric monoterpene emissions as a function of chemotype, light and temperature, Biogeosciences, 11, 1435–1447, https://doi.org/10.5194/bg-11-1435-2014, 2014.

Sorek-Hamer, M., Chatfield, R., and Liu, Y.: Review: Strategies for using satellite-based products in modeling $PM_{2.5}$ and short-term pollution episodes, Environ. Int., 144, 106057, https://doi.org/10.1016/j.envint.2020.106057, 2020.

Sparks, W. B., Hough, J., Germer, T. a, Chen, F., DasSarma, S., DasSarma, P., Robb, F. T., Manset, N., Kolokolova, L., Reid, N., Macchetto, F. D., and Martin, W.: Detection of circular polarization in light scattered from photosynthetic microbes, P. Natl. Acad. Sci. USA, 106, 7816–7821, https://doi.org/10.1073/pnas.0810215106, 2009b.

Sparks, W. B., Germer, T. A., and Sparks, R. M.: Classical Polarimetry with a Twist: A Compact, Geometric Approach, Publ. Astron. Soc. Pacific, 131, 75002, https://doi.org/10.1088/1538-3873/ab1933, 2019.

Stamnes, S., Hostetler, C., Ferrare, R., Burton, S., Liu, X., Hair, J., Hu, Y., Wasilewski, A., Martin, W., van Diedenhoven, B., Chowdhary, J., Cetinić, I., Berg, L. K., Stamnes, K., and Cairns, B.: Simultaneous polarimeter retrievals of microphysical aerosol and ocean color parameters from the "MAPP" algorithm with comparison to high-spectral-resolution lidar aerosol and ocean products, Appl. Opt., 57, 2394–2413, https://doi.org/10.1364/AO.57.002394, 2018.

Stamnes, S., Baize, R., Bontempi, P., Cairns, B., Chemyakin, E., Choi, Y.-J., Chowdhary, J., Hu, Y., Jeong, M., Kang, K.-I., Kim, S. S., Liu, X., Loughman, R., MacDonnell, D., McCormick, M. P., Moon, B., Omar, A., Roithmayr, C. M., Sim, C. K., Sun, W., van Diedenhoven, B., Videen, G., and Wasilewski, A.: Simultaneous Aerosol and Ocean Properties From the PolCube CubeSat Polarimeter, Front. Remote Sens., 2, 19, https://doi.org/10.3389/frsen.2021.709040, 2021.

Staudt, M., Byron, J., Piquemal, K., and Williams, J.: Compartment specific chiral pinene emissions identified in a Maritime pine forest, Sci. Total Environ., 654, 1158–1166, https://doi.org/10.1016/j.scitotenv.2018.11.146, 2019.

Tinoco, I. and Williams, A. L.: Differential Absorption and Differential Scattering of Circularly Polarized Light: Applications to Biological Macromolecules, Annu. Rev. Phys. Chem., 35, 329–355, https://doi.org/10.1146/annurev.pc.35.100184.001553, 1984.

Toth III, J. R., Rajupet, S., Squire, H., Volbers, B., Zhou, J., Xie, L., Sankaran, R. M., and Lacks, D. J.: Electrostatic forces alter particle size distributions in atmospheric dust, Atmos. Chem. Phys., 20, 3181–3190, https://doi.org/10.5194/acp-20-3181-2020, 2020.

Sascha, T.: POLARIZATION AND POLARIMETRY: A REVIEW, J. Korean Astronom. Soc. 47, 15–39, https://doi.org/10.5303/JKAS.2014.47.1.15, 2014.

Tsekeri, A., Amiridis, V., Louridas, A., Georgoussis, G., Freudenthaler, V., Metallinos, S., Doxastakis, G., Gasteiger, J., Siomos, N., Paschou, P., Georgiou, T., Tsaknakis, G., Evangelatos, C., and Binietoglou, I.: Polarization lidar for detecting dust orientation: system design and calibration, Atmos. Meas. Tech., 14, 7453–7474, https://doi.org/10.5194/amt-14-7453-2021, 2021.

Twohy, C. H., DeMott, P. J., Russell, L. M., Toohey, D. W., Rainwater, B., Geiss, R., Sanchez, K. J., Lewis, S., Roberts, G. C., Humphries, R. S., McCluskey, C. S., Moore, K. A., Selleck, P. W., Keywood, M. D., Ward, J. P., and McRobert, I. M.: Cloud-Nucleating Particles Over the Southern Ocean in a Changing Climate, Earth's Futur., 9, e2020EF001673, https://doi.org/10.1029/2020EF001673, 2021.

Tyo, J. S., Goldstein, D. L., Chenault, D. B., and Shaw, J. A.: Review of passive imaging polarimetry for remote sensing applications, Appl. Opt., 45, 5453, https://doi.org/10.1364/AO.45.005453, 2006.

Ulanowski, Z., Bailey, J., Lucas, P. W., Hough, J. H., and Hirst, E.: Alignment of atmospheric mineral dust due to electric field, Atmos. Chem. Phys., 7, 6161–6173, https://doi.org/10.5194/acp-7-6161-2007, 2007.

van de Hulst, H. C.: Light scattering by small particles, Dover Publications In, New York, New York: Dover Publications, Inc. 1981. Paperback, 470 S., 103 Abb. und 46 Tab., US, 1981.

Vandenbroucke, B., Baes, M., Camps, P., Utsav Kapoor, A., Barrientos, D., and Bernard, J.-P.: Polarised emission from aligned dust grains in nearby galaxies: Predictions from the Auriga simulations, Astro. Astrophys., 653, A34, https://doi.org/10.1051/0004-6361/202141333, 2021.

van der Laan, J. D., Wright, J. B., Kemme, S. A., and Scrymgeour, D. A.: Superior signal persistence of circularly polarized light in polydisperse, real-world fog environments, Appl. Opt., 57, 5464, https://doi.org/10.1364/AO.57.005464, 2018.

Van Eeckhout, A., Garcia-Caurel, E., Garnatje, T., Durfort, M., Escalera, J. C., Vidal, J., Gil, J. J., Campos, J. and Lizana, A.: Depolarizing metrics for plant samples imaging, edited by: Restani, P., PLoS One, 14, e0213909, https://doi.org/10.1371/journal.pone.0213909, 2019.

van Harten, G., Snik, F., Rietjens, J. H. H., Smit, J. M., de Boer, J., Diamantopoulou, R., Hasekamp, O. P., Stam, D. M., Keller, C. U., Laan, E. C., Verlaan, A. L., Vliegenthart, W. A., ter Horst, R., Navarro, R., Wielinga, K., Hannemann, S., Moon, S. G., and Voors, R.: Prototyping for the Spectropolarimeter for Planetary EXploration (SPEX): calibration and sky measurements, p. 81600Z, in: Proc. SPIE, 8160, p. 81600Z, https://doi.org/10.1117/12.893741, 2011.

Verdugo, P., Alldredge, A. L., Azam, F., Kirchman, D. L., Passow, U., and Santschi, P. H.: The oceanic gel phase: a bridge in the DOM–POM continuum, Mar. Chem., 92, 67–85, https://doi.org/10.1016/j.marchem.2004.06.017, 2004.

Videen, G.: Light Scattering Multipole Solution for a Cell, J. Biomed. Opt., 3, 212, https://doi.org/10.1117/1.429877, 1998.

Wang, X., Yao, G., and Wang, L. V.: Monte Carlo model and single-scattering approximation of the propagation of polarized light in turbid media containing glucose, Appl. Opt., 41, 792, https://doi.org/10.1364/AO.41.000792, 2002.

Wedyan, M. A. and Preston, M. R.: The coupling of surface seawater organic nitrogen and the marine aerosol as inferred from enantiomer-specific amino acid analysis, Atmos. Environ., 42, 8698–8705, https://doi.org/10.1016/j.atmosenv.2008.04.038, 2008.

Wei, X., Chang, N.-B., Bai, K., and Gao, W.: Satellite remote sensing of aerosol optical depth: advances, challenges, and perspectives, Crit. Rev. Environ. Sci. Technol., 50, 1640–1725, https://doi.org/10.1080/10643389.2019.1665944, 2020.

Westphal, P., Kaltenbach, J.-M., and Wicker, K.: Corneal birefringence measured by spectrally resolved Mueller matrix ellipsometry and implications for non-invasive glucose monitoring, Biomed. Opt. Express, 7, 1160, https://doi.org/10.1364/BOE.7.001160, 2016.

Whitney, B. A. and Wolff, M. J.: Scattering and Absorption by Aligned Grains in Circumstellar Environments, Astrophys. J., 574, 205–231, https://doi.org/10.1086/340901, 2002.

Williams, J., Yassaa, N., Bartenbach, S., and Lelieveld, J.: Mirror image hydrocarbons from Tropical and Boreal forests, Atmos. Chem. Phys., 7, 973–980, https://doi.org/10.5194/acp-7-973-2007, 2007.

Winker, D. M., Pelon, J., Coakley, J. A., Ackerman, S. A., Charlson, R. J., Colarco, P. R., Flamant, P., Fu, Q., Hoff, R. M., Kittaka, C., Kubar, T. L., Le Treut, H., Mccormick, M. P., Mégie, G., Poole, L., Powell, K., Trepte, C., Vaughan, M. A., and Wielicki, B. A.: The CALIPSO Mission, Bull. Am. Meteorol. Soc., 91, 1211–1230, https://doi.org/10.1175/2010BAMS3009.1, 2010.

Wood, M. F. G., Guo, X., and Vitkin, I. A.: Polarized light propagation in multiply scattering media exhibiting both linear birefringence and optical activity: Monte Carlo model and experimental methodology, J. Biomed. Opt., 12, 014029, https://doi.org/10.1117/1.2434980, 2007.

Yassaa, N., Brancaleoni, E., Frattoni, M., and Ciccioli, P.: Trace level determination of enantiomeric monoterpenes in terrestrial plant emission and in the atmosphere using a beta-cyclodextrin capillary column coupled with thermal desorption and mass spectrometry., J. Chromatogr. A, 915, 185–197, https://doi.org/10.1016/S0021-9673(01)00587-8, 2001.

Yassaa, N., Peeken, I., Zllner, E., Bluhm, K., Arnold, S., Spracklen, D., and Williams, J.: Evidence for marine production of monoterpenes, Environ. Chem., 5, 391–401, https://doi.org/10.1071/EN08047, 2008.

Zeng, X., Chu, J., Cao, W., Kang, W., and Zhang, R.: Visible–IR transmission enhancement through fog using circularly polarized light, Appl. Opt., 57, 6817–6822, https://doi.org/10.1364/AO.57.006817, 2018.

Zhang, H. and Zhou, Y.-H.: Effects of 3D electric field on saltation during dust storms: an observational and numerical study, Atmos. Chem. Phys., 20, 14801–14820, https://doi.org/10.5194/acp-20-14801-2020, 2020.

Zhou, Y., Levy, R. C., Remer, L. A., Mattoo, S., and Espinosa, W. R.: Dust Aerosol Retrieval Over the Oceans With the MODIS/VIIRS Dark Target Algorithm: 2. Nonspherical Dust Model, Earth Sp. Sci., I7, e2020EA001222, https://doi.org/10.1029/2020EA001222, 2020.